Master Dissertation in Mechanical Engineering

Analysis of the effects of Shading over a PV system: MPPT under periodic Partial Shading Conditions

Author:
Patrick James Welsh Talas

Supervisor:
Prof. Joaquim Gabriel Magalhães Mendes
Eng. Miguel Marques

Specialization in: Masters degree in Mechanical Engineering

March, 2022

Acknowledgements

This dissertation has been made possible thanks to my supervisor prof. Joaquim and co-supervisor eng. Miguel, my father Jorma and one of my childhood and best friends mum, Kim. I would also like to thank my family and my friends who have been on this journey with me. A special thank you to all.

Abstract

In this dissertation the topic of dynamic shading on PV modules and systems are analysed. Dynamic shading can come from clouds or from objects in the environment which may interfere momentarily with the production of power. To study this effect, this dissertation proposes to simulate a PV system composed of a module and a converter for a step function whose amplitude is 1000 W/m^2 when fully irradiated and non existing when under the shading condition for one section of the module covered by a bypass diode. In order to maximise the power generation, three algorithms for tracking the maximum power point are compared in terms of their behavior, along with the parameters of the converter and adjustment of the duty cycle. The perturb and observe MPPT algorithm, the conventional incremental conductance algorithm and a modified version of the latter. In terms of performance under fully illuminated conditions, the PO was able to generate more power to the load for the conditions simulated, while it failed to make an accurate judgment on the maximum power under the shaded interval. Conversely, the conventional INC algorithm fails to make a good decision when the irradiance suddenly increases. With these algorithms the power plateaus at a lower power but is able to generate more power than the perturb and observe algorithms. The modified incremental conductance algorithm seems to behave in a reliable and accurate manner under rapidly changing irradiation.

Resumo

Esta dissertação aborda o tema do sombreamento dinâmico em módulos e sistemas fotovoltaicos. O sombreamento dinâmico pode vir de nuvens ou de objetos no ambiente que podem interferir momentaneamente na produção de energia. Para estudar este efeito, esta dissertação propõe simular um sistema fotovoltaico composto por um módulo e um conversor para uma função degrau cuja amplitude é de 1000 W/m^2 quando totalmente irradiado e inexistente quando sob a condição de sombreamento para uma seção de o módulo coberto por um diodo de bypass. Para maximizar a geração de energia, três algoritmos de rastreamento do ponto de máxima potência são comparados quanto ao seu comportamento, juntamente com os parâmetros do conversor e de ajuste do ciclo. O algoritmo *Perturb and Observe* ($P\&O$), o algoritmo convencional de condutância incremental (IC) e uma versão modificada deste último. Em termos de desempenho nas condições totalmente iluminadas, o $P\&O$ foi capaz de gerar maior potência para a carga para as condições simuladas, enquanto não conseguiu fazer um julgamento preciso da potência máxima sob o intervalo sombreado. Por outro lado, o algoritmo IC convencional não consegue tomar uma boa decisão quando a irradiância aumenta repentinamente. Nestes algoritmos a potência estabiliza num valor menor durante estas condições, mas é capaz de gerar mais potência do que os algoritmos $P\&O$ quando sombreado. O algoritmo de condutância incremental modificado parece se comportar de maneira precisa e mais exacta perante a condição de sombreamento dinâmico empregue.

"Antifragility is beyond resilience or robustness. The resilient resists shocks and stays the same; the antifragile gets better. "

— Nassim Nicholas Taleb, Antifragile: Things That Gain from Disorder

Contents

Contents vi

List of figures ix

List of figures xi

1 Introduction 1
- 1.1 Purpose . . . 1
- 1.2 INEGI . . . 1
- 1.3 Methodology . . . 1
- 1.4 Dissertation Outline . . . 2
- 1.5 Background . . . 2
- 1.6 Hybrid Wind and Solar Parks . . . 3
  - 1.6.1 Effective utilization of land and renewable energy resources 4
  - 1.6.2 Savings on grid connecting system, common infrastructure cost and operating costs due to shared services . . . 4
  - 1.6.3 More balanced power generation for sale . . . 5
  - 1.6.4 Shading effect . . . 6

2 Solar cells 9
- 2.1 Solar cells . . . 9
  - 2.1.1 Bond and Band Model . . . 10
  - 2.1.2 Intrinsic and Extrinsic Semiconductors . . . 11
  - 2.1.3 PN junction . . . 11
  - 2.1.4 Solar Cells . . . 12
- 2.2 Silicon Solar Cells . . . 13
- 2.3 The Irradiation . . . 13
- 2.4 Absorption coefficient . . . 15
- 2.5 The Band Gap . . . 17
- 2.6 Recombination . . . 18
  - 2.6.1 Radiative (Band-to-Band) Recombination . . . 19
  - 2.6.2 Recombination Through Defect Levels . . . 19
  - 2.6.3 Auger Recombination . . . 19
- 2.7 The breakdown effect . . . 19

3 Literature Review 21

3.1 Shading on PV modules . . . 21
3.2 Grid Connection . . . 24
3.3 Optimisation . . . 26
3.4 Visualization and quantitive analysis . . . 29

4 Mathematical Modeling of a PV cell and module 31
4.1 The 5 Parameter Model . . . 31
4.1.1 Qualitative parameters . . . 33
4.1.2 I-V Characteristics of Junction Diodes . . . 34
4.1.3 Effect of series resistance . . . 34
4.1.4 Effect of shunt resistance . . . 35
4.1.5 Effect of Temperature . . . 35
4.1.6 Effect of Ideality factor: . . . 36

5 DC converter 37
5.1 DC-DC Converters . . . 37
5.2 Active Power Control . . . 39
5.3 Max Power Point Tracking Algorithms . . . 40
5.3.1 Perturb and Observe Algorithm: . . . 40
5.3.2 Incremental Conductance . . . 42
5.3.3 Modified Incremental Conductance . . . 43

6 Model Construction and case descriptions 45
6.1 Construction of the Models . . . 45
6.2 Case Description: . . . 47

7 Simulation Results 51
7.1 Results . . . 51
7.1.1 Case 1.0 . . . 51
7.1.2 Case 2.0 . . . 54
7.1.3 case 3.0 . . . 57
7.2 Discussion . . . 61

8 Conclusion 63
8.1 Conclusion . . . 63
8.2 Future Work . . . 64

List of Figures

1.1 Hybrid wind and solar park in South Korea [1] 3
1.2 Example of an interesting complementary wind and solar resource measured in terms of the capacity factor in the vertical axis [2] 6

2.1 Theoretical solar cell efficiency as a function of the energy gap [3] 10
2.2 PN Junction [4] 12
2.3 Solar cell composition [5] 13
2.4 Spectral response of different materials along with the AM1.5 G up to 1300nm [6] 14
2.5 Spectral response of different materials [3] 15
2.6 Absorption coefficient for different materials [7] 16
2.7 Simplified energy band diagram for direct band gap materials at T>0 K [8] 17
2.8 Simplified energy band diagram for Indirect band gap materials at T>0 K. Energy and Momentum are conserved by the absorption or emission of phonons [8] 17
2.9 I-V characteristical curve for a typical diode [9] 20

4.1 Equivalent 5 parameter electrical circuit [10] 31
4.2 Visual representation of the essential contributing parameters for mapping the I-V characteristic load represented in equation 4.1, from ref[3]. 32
4.3 Definition of Fill Factor in the I-V curve [11]. 33
4.4 I-V characteristic of a diode 34
4.5 Effect of altering either the series resistance or the shunt resistance in the I-V characteristic curve [12] 35
4.6 Effect of Temperature increase on the I-V characteristic curve [7] 36

5.1 Electric circuit of a boost converter [10] 37
5.2 Voltage ripple [13] 39
5.3 Representation of the operating area of the system under the I-V characteristic curve for different operating conditions [14] . . 40
5.4 Perturb and Observe flowchart 41
5.5 IC flowchart [15] 42
5.6 Modified IC flowchart [16]. 43

6.1 Solar cell blocks each representing 48 cells in series connected in parallel with the bypass diode 4.1. 45
6.2 Solar Module (3×48 cells) in series connected to 46
6.3 Full sized model of the system. Each subsystem includes one module and a boost converter configuration. 6.2 46

7.1 I-V characteristic curve for different levels off uniform irradiance 51
7.2 P-V characteristic curve for different levels of uniform irradiance 52
7.3 I-V characteristic curve for different levels of non uniform irradiance 53
7.4 P-V characteristic curve for different levels of non uniform irradiance, case 1.0 a) and f) through k) 53
7.5 Model used for case 1.0. On the left side, the P-V graphs for the cases of uniform 1000 W/m^2 and the case 1000-1000-0 W/m^2 illustrate the variation of the characteristic curve if shading of one submodule takes place. On the right the model used to simulate case 1.0 54
7.6 Power output vs time for different loads under dynamic shading of 1 subsection of 1 module 54
7.7 Power output vs time for different loads under dynamic shading of 1 subsection of 1 module 55
7.8 Changes to the magnitude of the power output signal for different values C_{in} $[\mu F]$ and a fixed duty cycle under periodic shading 55
7.9 Changes to the ripple of the power signal for different values of C_{out} and a fixed duty cycle under periodic shading 56
7.10 Changes to the magnitude of the power signal for different values of the inductor resistance and a fixed duty cycle under periodic shading 56
7.11 Changes to the output power signal for different values of C_{out} resistance and a fixed duty cycle under periodic shading. 57
7.12 Changes to the magnitude of the power signal for different conductance values of the diode and the switch values and a fixed duty cycle under periodic shading 57
7.13 Simulation results of P&O algorithm under different duty ranges, step sizes and loads 58
7.14 Simulation results of I.C. algorithm and further adjustment of converter 58
7.15 Simulation results for the Incremental Conductance algorithm . 59
7.16 Simulation results of the Incremental Conductance algorithm: adjustment of the converter parameters 59
7.17 Simulation results of Modified Incremental Conduction, for different duty cycles 60
7.18 Simulation results of Modified Incremental Conduction, for different step sizes 60

7.19 Close up view to the response for different step sizes 60

List of Tables

5.1 Summary of the action of the Perturb and Observe algorithm [15] 41
5.2 Summary of the action by the Incremental Conduction algorithm [15] 43

6.1 Solar cell block parameters 47
6.2 Module boost converter parameters 47
6.3 Boost converter parameters used for I.C. 47
6.4 Case description for static conditions simulation 48
6.5 Case description for dynamic conditions simulation 48

7.1 Summary of results obtained by shading one module under uniform and non-uniform irradiation 52

Chapter 1
Introduction

1.1 Purpose

As different sources of renewable energies are being investigated and championed for hybrid purposes, combining wind turbines with photovoltaics (PV) doesn't come without some limitations. The aim of this dissertation is to investigate and create a general level of knowledge into the effects of shading on PV modules and PV strings. By creating a model for simulation and applying a dynamic maximum power point tracking system, the effect and limitations these may have in mitigating the shadow, current mismatch, and power output are investigated for a periodic step like shading condition

1.2 INEGI

INEGI - Institute of Science and Innovation in Mechanical Engineering and Industrial Engineering is a technological interface center, created in 1986 oriented towards the research and development of innovative technologies, consultancy and services in industry. Their mission is to aid in the development of industry by developing projects tailored to the needs of both customers and partners. In terms of issues connected to renewable energies, the environment and sustainability, INEGI offers the possibility to model, characterise, prototype and monitor, in face of different production scenarios, different energy conversion systems such as hydro, tidal, wave, biomass and in particular to this project, wind and solar energy conversion systems.

1.3 Methodology

In this dissertation in order to study the effects of shading on PV systems, it is proposed to first conduct research behind the phenomena to then create and simulate a model, using MatlabR2020a, for shade mitigation by implementing a max power point tracking algorithm and investigating the reaction of the system towards a periodic "on","off" shadow.

1.4 Dissertation Outline

This dissertation is divided into 8 chapters.

The first chapter discusses hybrid wind and solar parks, presenting some of the benefits these distributed generating systems may have and a small overview of the effect of shading on the PV system and on the land. In chapter 2 the theory behind the operation mechanism in solar cells are briefly analysed. In chapter 3, the literature review presents an overview, regarding the effects of shading over cells and systems and different optimisation techniques available. In chapter 4 a mathematical model for PV cells is defined based on literature and the effects of its parameters are briefly discussed. Chapter 5 presents the model for the boost converter and two different MPPT algorithms. In chapter 6 the Simulink model is presented and the cases for simulation are described In chapter 7 the simulations are performed and the results displayed. In this chapter result discussion also takes place, and the effect MPPT algorithms under the imposed shading conditions are analysed and effects discussed. Chapter 8 concludes the findings of the simulation and in literature and presents future scopes.

1.5 Background

Fossil fuels are the leading source of power in our society. The ever-increasing demand for sustainable clean energy, along with green technologies is transforming the traditional fossil fuel demand into a renewable energy source. Environmental issues, with concerns on the emission of greenhouse gases, climate change and the depletion of natural reserves such as oil, natural gas, and coal, is motivating research and investment into renewable energy sources. In 2015, for the first time, almost every country around the world committed to reduce emissions under the Paris Agreement at COP21. Ambitious goals were set out to adapt and finance these measures, recognising that many people around the world were already suffering, to some degree, the impacts of the changing climate [17]. In order to meet these goals, financial, technical, and support infrastructures were needed. To encourage the financial sector to do more, the COP Presidency, the UN High Level Climate Champions and the President of the Bank of England, launched the Glasgow Financial Alliance for Net Zero (GFANZ) to reduce greenhouse gas emissions. This already unites over 160 firms, who together are responsible for assets in excess of US70 trillion dollars, leading net zero initiatives across the financial system to accelerate the transition to net zero emissions by 2050 at the latest [18]. More recently, during COP 26, there was an inflection point for increased action regarding fossil fuels and renewable energies calling on countries to “revisit and strengthen” their 2030 targets [19]. Governments agreed on Nationally Determined Contributions (NDCs) on CO2 and methane emission reductions as well as financing poorer countries towards this change. The needs of poorer

communities, as well as social and economic inclusion for underprivileged and threatened groups, through development, was highlighted as a priority. Energy availability is often one of the keys towards this objective. US100 Billion Dollars have already been pledged as a minimum for investment initiatives for sustainable projects and research for national emission reduction targets to limit the temperature increase to 1.5 degrees Celsius [19]. Renewable energy sources are today an unquestionable part of the definition of energy policy, which ranges from macro planning, at national and community levels, to the domestic level. [18].

1.6 Hybrid Wind and Solar Parks

Figure 1.1: Hybrid wind and solar park in South Korea [1]

The further development of renewable energy sources involves research and investment into hybrid solutions, amongst others. Wind and solar have grown dramatically in the past few decades, along with advances in hybrid technology, expanding the possibilities of generating electricity. On average for the last five years, 24% of electricity consumption in Portugal came from wind turbines [2], which makes hybrid generation particularly interesting. Hybrid energy parks can be considered relevant in confined spaces, as well as remote areas, and where both wind speed and solar irradiance undergo big weekly fluctuations. It becomes especially important when one source on its own isn't enough to power the demand, as in poorer communities. Regions without electricity need to be able to increase and sustain consistent energy production and useability. Solar energy and wind energy have characteristics that, depending on the interday and intraday cycles, enhance their complementarity, and may have advantages compared to their individual and separate use [20].

Wind-solar hybrid projects offer several operational synergies, leading to long-term savings in capital investments, operation and transmission of power

from hybrid plants. The complementary generation patterns lead to more balanced generation curves, with less variability, by reducing peak to average ratio for power generated, and thus ensure a stable and robust injection in the grid. Combining both technologies generally improves the capacity to respond to the load profile. This allows projects to adhere to stringent scheduling and forecasting guidelines, without any penalties or duties to be paid for non-adherence to statutory compliance [20]. In addition, the support of energy storage systems also helps mitigate the mismatch between load and generation profiles.

Electricity generation from wind turbines is generally a thousand times greater than from photovoltaics. However, it is very site-specific, whereas photovoltaics are generally applicable to most locations. Wind turbines are usually placed at large distances from each other in a typical wind farm, resulting in wastage of large tracts of land. Unused land can be better utilised by installing solar panels in the shadow-free area available around wind turbines, adding to the generation of energy.

Maximising energy generation from the land, while minimising the levelized cost of energy have been cited as the most important goals by investors at present [20]. Key benefits of wind-solar hybrids are diversification of resources due to spatial distribution of renewable energy generators. Incorporating different technologies to meet energy demands, improves predictability of power generation and more balanced generation curves and reduce investments in energy storage. This also optimises delivery for load matching, scheduling, transmission cost, and higher ability to meet more stringent norms for grid interconnection (control over power injection, voltage, etc.). [20]

1.6.1 Effective utilization of land and renewable energy resources

In Europe, empty land available for solar and wind projects might become a major limitation in the future and land costs and acquisition challenges will also keep increasing. Therefore, land resources should be used effectively to ensure maximum generation. It has been estimated that energy generation per unit area of land, in the case of a large-scale hybrid zone will be significantly higher compared to an only wind/solar scenario. [20]

1.6.2 Savings on grid connecting system, common infrastructure cost and operating costs due to shared services

Wind and solar have completely independent and complementary generating patterns. In projects where wind or solar capacity is less than 30% of total, the smaller capacity can ride free on the evacuation capacity created for the larger capacity. Typically, wind power generation picks up after sunset and

reaches its peak generation late night, thereby effectively utilising the power evacuation infrastructure and saving costs. By sharing the same evacuation systems, it is possible to deliver more power to the grid without additional investments, making use of the idle capacity of this asset. Other infrastructure such as roads, plant control, spares warehousing, energy storage, forecasting and scheduling may be created cost effectively and shared. Operations and maintenance schedules can be optimised for best utilisation of non-operating and lean hours for routine maintenance work without losing out on generation, as would be the case in a pure solar or wind project. Further, once the team appointed at site are familiar with the workings of both wind and solar, a very lean and highly experienced team can carry out electrical and civil maintenance works, effectively saving on manpower and material cost (of keeping two separate teams) on an annual basis. Services such as administration, security, accounting, forecasting and scheduling can also be shared and result in reduced costs. [20]

1.6.3 More balanced power generation for sale

For choosing an optimised capacity mix of solar and wind for a hybrid plant, it is imperative to take the variability of energy generation from the hybrid plant into consideration [2]. It can be ascertained from the peak to average energy generation ratio and coefficient of variation of energy generation from the resultant hybrid. The hybrid plant can bring the peak energy curve closer to average energy curve and ensure the least variability in generation from the average generation, with a lesser ratio of peak to average power for the same hour throughout the year than if wind or solar is taken separately.[20]

Balancing both energy sources can be difficult, since each has a distinct generation profile and both suffer in terms of availability and intensity variations over time and in geographic space [2]. The capacity, location and intra-day cycles are key factors. It is necessary to verify the degree of complementary between the two, case by case. A high simultaneity of resources may hamper the performance of the hybrid power plant when energy storage systems are insufficient or non-existing.

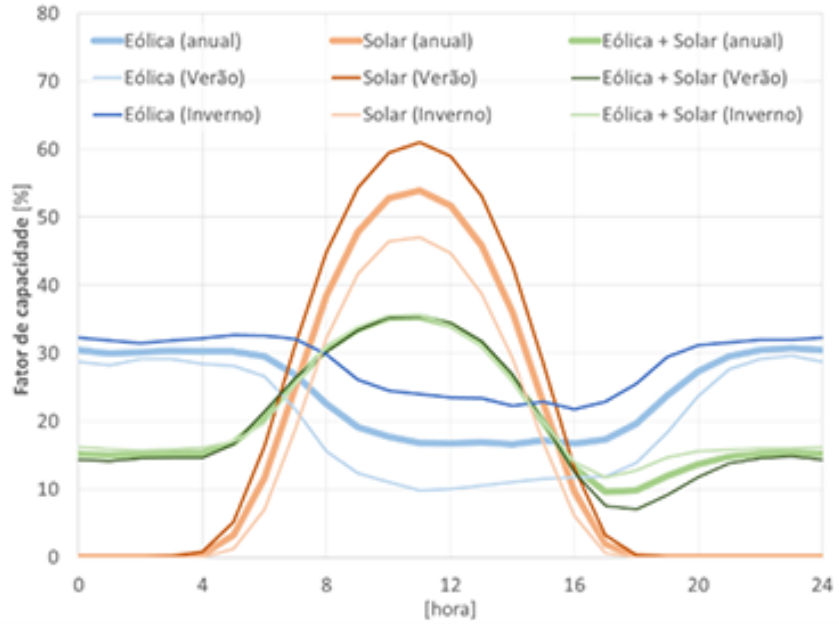

Figure 1.2: Example of an interesting complementary wind and solar resource measured in terms of the capacity factor in the vertical axis [2]

In figure 1.2, an example case study from reference [2] is illustrated and presents the average intraday capacity factor for both wind and solar resources for the summer and the winter season and annualy. It can be seen that the intra-annual variability of the wind resource is not significantly pronounced from summer to winter. But the intraday variability is sufficient to make for interesting conditions for complementary production.

1.6.4 Shading effect

Mamia, I. and Appelbaum, J. 2016 [21]investigate the shadow cast by wind turbines by calculating the invasion on the land area they impose during the year for two latitudes, 32° and 50°. The calculations show that the average percentage loss of land due to this phenomena is less than one percent. Typical turbine spacing in wind farms is placing the towers 5 rotor diameters in the crosswind direction and roughly 10 rotor diameters in the downwind direction [21]. The shadow cast by a turbine may be of the order of a few hundred square meters, invading neighboring tower ground area mostly in the morning and in the afternoon hours. It was found that for a latitude of 32°, no shadow invasion occurred for more than 7h in the entire year. While for a latitude of 50° no shadow invasion occured for more than 6 h during a day in a year for most months [21]. However, in November, December and January, for a latitude of 50°, invasion to neighboring tower area occurs for the whole day [21], therefore an appropriate shadow analysis must take place in order to appropriately understand the invasion and mitigate its effects on PV systems.

Hot spot heating occurs when there is one low current solar cell in a

string of at least several high short-circuit current solar cells.[20] It occurs when electrons accumulate in cell and heat surge is experienced as the cell starts to act like a resistor. It results in lower power output and accelerated degradation of materials in the area. This happens when sharp and persistent shadows affect a few cells. Wide shadows, moving shadows and shadows in low light conditions (evenings or mornings) are likely to result in very little to no hot spotting [20]. Therefore, in a wind-solar hybrid park, the solar modules should be placed in a manner that no shadow falls on them between the times of highest energy production. When the generation from solar is low, the impact on the PV modules isn't as harmful and therefore the likelihood of hot spots will also be low [20]. In addition to turbine tower shadow, shadow flicker occurs due to rotation of wind turbine blades and cause shadows to flick on and off, resulting in periodic and fast changes in light intensity. These shadow flickers may cause frequent alternation in light intensity and affect the PV power output. Fast moving clouds on photovoltaic panels may cause fluctuations and flickers in output power similar to the rotating turbine blades [22].

When considering the height of the blades, the shadow invasion of a turbine to the neighbouring turbine area is more pronounced. The area it covers represents a loss of land around 1% to 2%. Considering the Nacelle and Hub dimensions, their shadows may add about 5 percent to the total shaded area of the turbine, thus their shadow effect remains still negligible [21].

Taking into account the need for land for the turbine tower bases, crane pads, access roads, substations and service buildings, there is still ample area for PV systems. A question then remains is the impact of fast moving shadows by the blades on the inverter operation. As dynamic methods for mitigating shadow effects and flickers by electronic means are incorporated in today's inverters, one may assume that shadows do not pose an obstacle in sharing the wind land for solar power generation[21]. Recent advancements in inverter technology with provisions of dynamic maximum power point tracking (MPPT) make it possible to track and quickly adjust the voltage levels for maximum power.

Chapter 2
Solar cells

2.1 Solar cells

Solar cells are manufactured from semiconductor materials due to their capacity to generate a current. Most solar cells are made from silicon. The electronics industry has been at the forefront and of research and technology in extracting the benefits crystalline silicon cells. Although it has been known since the 1950's that other semiconductors make good solar cells, silicon solar cells are currently the cheapest method for mass production with good cost benefit ratios. Other semiconductors are being researched which may supersede silicon in the long term for commercial use [3]. For example, the best efficiency obtained for a single-junction solar cell was with Gallium Arsenide (GaAs) research-type cells reaching 27.6% efficiency, although, it was achieved by concentrating sunlight to that of 255 suns (255 kW/m^2). Typical commercial silicon cell efficiency is around 15% for standard conditions (1 kW/m^2). The maximum efficiency that can be obtained from a single junction solar cell is theoretically around 40% under optimal conditions [8]. Also the idea of surface texturing of the solar cell to reduce the optical reflection losses and maximise the number of photoactive photons absorbed are being explored, [23]. Record-breaking efficiency of Si solar cells of 26.6% have been achieved in this manner. To further improve the efficiency closer to the theoretically possible, which is near 29%, requires a better consideration, in particular of the recombination mechanisms in silicon. This should include the non-radiative recombination via deep impurity centres and the recombination in the space-charge region [23]. Another way to attempt to extract more power is through stacking cells with different band gap layers with higher band gap materials stacked at the top and lower band gap materials at the bottom. Semiconductors with higher band gaps allow for higher intensity photons to be absorbed at the top and to generate more power while the photons with less energy than the top cells band gap penetrate through these layers and get absorbed further in by layers with lower band gaps. The limit efficiency, with an infinite number of cells stacked with different band gaps is about 86%, as compared to 40% for the single band gap cells. In reality, efficiencies up to 32% have been achieved for a three band gap stacked cells of GaInP/GaAs/Ge, (Indium Gallium Phosphide/ Gallium

Arsenide/ Germanium), under standard conditions. While efficiencies up to 26% with a single band gap GaAs solar cell and of over 29% with a double band gap GaInP/GaAs cells have also been achieved. Thin film cells are another form of producing cells which can be employed for multi-layered usage. However, they may also be used on their own. Regarding thin film solar cells, (TFSC), amorphous silicon cells are the most common, however polycrystalline layers of Cu(InGa)Se2, (Copper Indium-Gallium Selenium), alloys have produced the highest efficiency devices and modules. TFSCs based on CuInSe2 (without Ga) are known to be 12% to 15% efficient however they are limited by the low band gap. Therefore, by alloying it with Ga increases the band gap and increases the efficiency of delivering the electrons to the circuit [8].

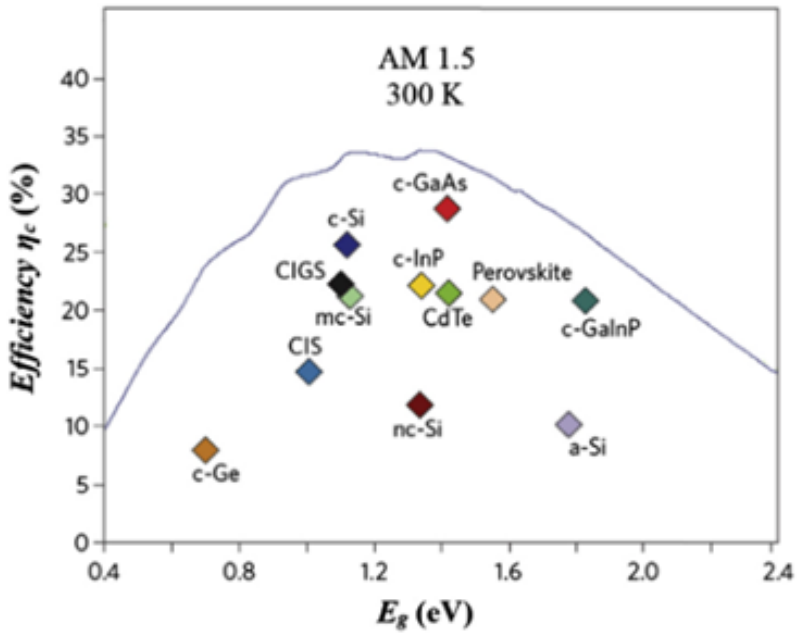

Figure 2.1: Theoretical solar cell efficiency as a function of the energy gap [3]

2.1.1 Bond and Band Model

According to the bond model, semiconductors, at low temperatures, act as an insulator thanks to the intact bonds joining the silicon atoms. As the material gains energy or heats up, some of these bonds begin to break and the electrons free themselves. Electrons from the broken bond move, leaving behind a hole. The neighbouring bonds may move to the broken bond, allowing the broken bond to propagate as if it had a positive charge. According to the band model, the electrons connected to the nucleus in covalent bonds have energies corresponding to those in the valence band. In the conduction band the electrons are free. The minimum energy needed to release an electron from a covalent bond to the conduction band is known as the band gap. The holes

remaining conduct in the opposite direction in the valence band, as described for the bond model. In the presence of an external circuit and an electric field the electrons get further energised and excited, jumping to the conduction band. The movement of the electrons in the external circuit and contacts is called the electric current.

2.1.2 Intrinsic and Extrinsic Semiconductors

It is common to distinguish two types of semiconductors. intrinsic semiconductors and extrinsic semiconductors. Intrinsic semiconductors have electrical properties determined by the properties of the underlying crystalline structure. The intrinsic carrier concentration is the number of electrons in the conduction band or the number of holes in the valence band in intrinsic material. Extrinsic semiconductors on the other hand are doped with elements whose characteristics are different from the underlying crystalline structure, in the order of 100 to 1000 parts per million. An n-type semiconductor, also known as an electron membrane, is one which has been doped with an element that confers a large electron conductivity with respect to the hole conductivity, namely by a large difference in electron and hole concentrations. Electrons can easily flow through the n-type semiconductor while the transport of holes, which are the minority carriers in such material, are very limited due to the recombination processes. In this case, the element is considered weakly connected and its electrons have superior energy levels compared to those electrons which are connected in the underlying structure, whose energy levels are close to the minimum absolute value of the energy in the conduction band. The opposite holds for electrons in a p-type semiconductor, which is an example of a hole membrane. Holes can easily flow through the p-type semiconductor while the transport of electrons is very limited.[24]

2.1.3 PN junction

The PN junction in thermal equilibrium has no net current flow. Since there is a concentration difference of holes and electrons between the two types of semiconductors, holes diffuse from the p-type region into the n-type region and, similarly, electrons from the n-type material diffuse into the p-type region. The transition region between the n-type and the p-type semiconductors is called the space-charge region. It is also often called the depletion region, since it is effectively depleted of both holes and electrons. Assuming that the p-type and the n-type regions are sufficiently thick, the regions on either side of the depletion region are essentially charge-neutral (quasi-neutral). The opposition that takes place in the p-region which becomes depleted of holes and the depletion of electrons on the n-region results in the electrostatic potential difference of the junction, called the built-in voltage. [24]

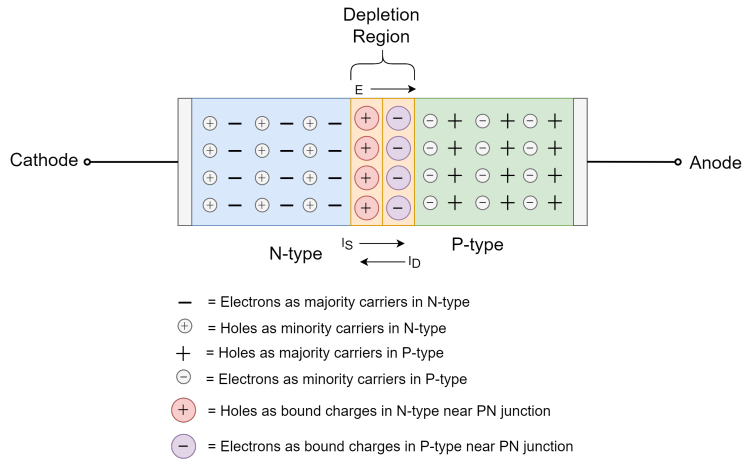

Figure 2.2: PN Junction [4]

By connecting an external DC voltage, biasing of the PN Junction diode depends upon the polarity of the DC voltage to the terminals of PN diode. The biasing may be forward biased, reverse biased or zero biased. When the positive terminal is connected to the p-type and the negative terminal is connected to the n-type, the solar cell is forward biased. Else, if the positive terminal is connected to the n-type and the negative terminal is connected to the p-type, then the solar cell is reverse biased. if no voltage is applied to the PN Junction, then it is zero biased.

2.1.4 Solar Cells

A solar cell is essentially a photodiode made by joining the p-type and n-type silicon. When the cell is exposed to light the photovoltaic effect takes place. In general, the photovoltaic effect means the generation of a potential difference at the junction of two different materials in response to radiation.[3] The photovoltaic effect can be divided in three basic processes:

- Generation of charge carriers (electron-hole) by absorption of photons in the photoelectric layers of the device
- Separation of the photo-generated charge carriers in the junction
- Collection of the photo-generated charge carriers at the terminals of the junction.

Semiconductors absorb light and deliver a portion of the energy of the absorbed photons to carriers of electrical current – electrons and holes. The electrical-charge carrier pairs are generated by absorbing photons. When these photons hit the valence electrons, if the incoming energy exceeds the band gap

energy, the bonds that tie the valence electrons to the material are broken and the electron jumps to a new energy band called the conduction band. Here, the electrons can conduct electricity through the material. Under the influence of the internal electric fields of the p-n junction, these carriers are swept apart and are collected, generating electrical current with a preferential direction and directly proportional to solar insolation [8].

2.2 Silicon Solar Cells

The structure of a silicon solar cell is composed of a metallic grid, at the top and at the bottom, forming the negative and the positive contacts respectively. An anti-reflective glass layer, which increases the amount of light absorbed and both an n-type layer and a p-type layer that form the diode junction. There are mainly three types of silicon cells: mono-crystalline, multi-crystalline and amorphous cells. For mono crystalline silicon solar cells, the atoms are arranged in a regular pattern forming a single crystal. The manufacturing process is rather slow and requires a lot of care, making this solar cell more expensive than its counterparts. For Multi-crystalline or polycrystalline silicon, the crystalline Si structure is made up of multiple crystals separated by irregular boundaries. It is cheaper to produce since the techniques are less critical. Amorphous silicon cells are the cheapest of the silicon based cells to produce, since there is no long-range order in the structural arrangement of the atoms, it is more irregular [8].

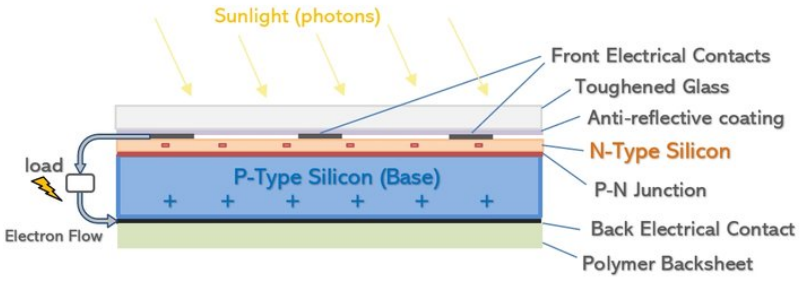

Figure 2.3: Solar cell composition [5]

2.3 The Irradiation

Sunlight is a spectrum of photons distributed over a range of energy. Only those photons emitted directly in the direction of the Earth contribute to the solar spectrum as observed from Earth. Both the intensity of the solar radiation reaching the Earth's surface and absorption in the atmosphere affects the spectral content. The spectral distribution is referred to as air mass and can be calculated by equation 2.1, by measuring the zenith angle, θ. It measures how absorption in the atmosphere affects the spectral content and intensity

of the solar radiation reaching the Earth's surface. Just above the Earth's atmosphere, the air mass is known as air mass zero $[AM_0]$ and the the radiation intensity, or Solar Constant, is about 1.353 $[kW/m^2]$ [7].

$$AM = 1/cos(\theta) \tag{2.1}$$

.

A widely used standard for comparing solar cell performance is the AM1.5 spectrum normalized to a total power density of 1 $[kW/m^2]$. The spectral content of sunlight at the Earth's surface also has a diffuse (indirect) component owing to scattering and reflection in the atmosphere and surrounding landscape and can account for up to 20% of the light incident on a solar cell. Different materials have different responses to the amount of light it can capture to generate power. The Spectral response of a PV device is given by the probability that the absorbed photon will yield a carrier to the photogenerated current of the cell I_{p_h}.

It is a function of the band gap, cell thickness and diffusion of electrons in the material. It measures the ratio of the current to incident solar power on its surface. For short wavelengths the spectral response is lower since each photon has a large amount of power and a very small probability of colliding with two electrons simultaneously (if it is a direct process). Figure illustrates the spectral response of silicon cells and copper indium selenide cells along with the AM1.5 G (global air mass) spectrum for comparison and figure illustrates the response for different materials, respectively.

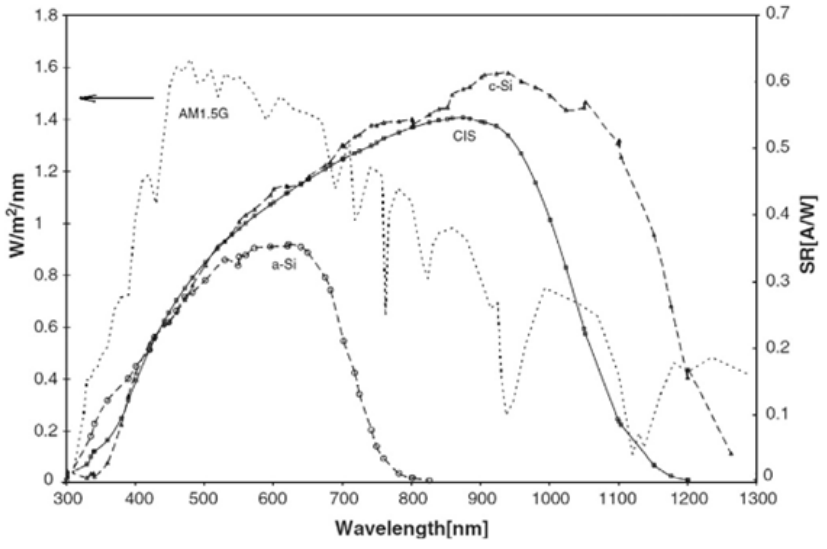

Figure 2.4: Spectral response of different materials along with the AM1.5 G up to 1300nm [6]

Photons that fail to be absorbed instead travel through the solar cell and are collected as heat in the rear. In practical conditions the actual solar radiation varies according to; the position on the earth, the month of the

year, the day and time, the presence of clouds in the air mass and other environmental effects, the angle of incidence which depends on the positioning of the panel relative to the sun, and the presence of other external factors which may also produce shade.

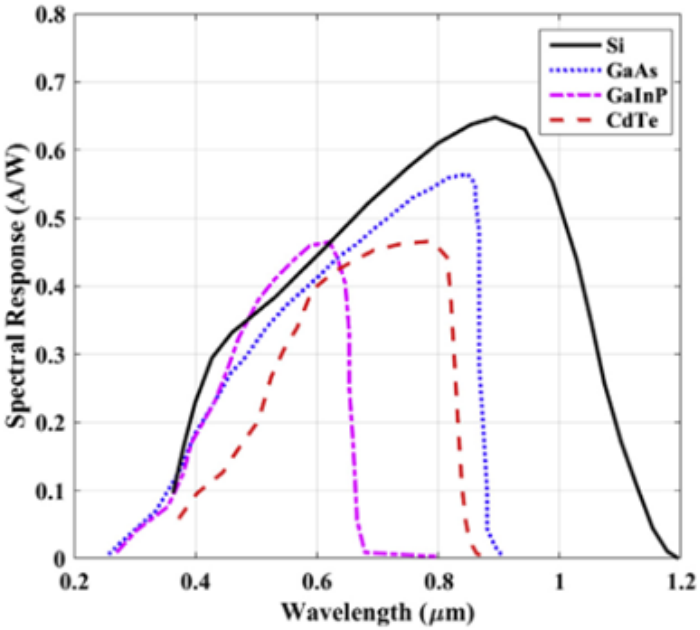

Figure 2.5: Spectral response of different materials [3]

2.4 Absorption coefficient

Different semiconductor materials have different absorption coefficients. It determines how far into a material a given wavelength of light can penetrate before it is absorbed. A higher absorption coefficient means the material absorbs photons and excites electrons into the conduction band with greater ease and in shorter distance. The absorption coefficient depends on the wavelength of light which is being absorbed, as can be seen by figure 2.6 where larger wavelengths correspond to photons with lower energy.

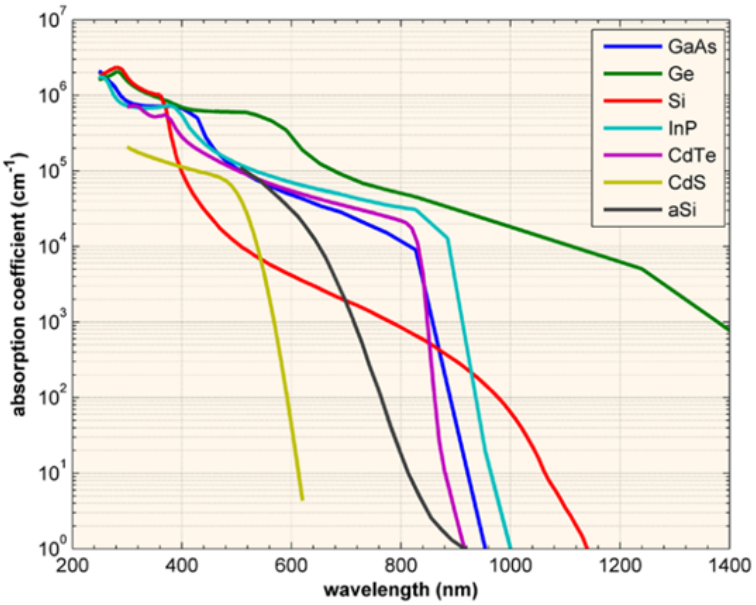

Figure 2.6: Absorption coefficient for different materials [7]

As the wavelength increases, the depth the light penetrates before it's absorbed increases, which decreases the absorption coefficient. For photons with an energy very close to the band gap, absorption is relatively low since only electrons directly at the valence band edge can interact with the photon, each photon has fewer electrons to interact with. By increasing the photon's energy (shorter wavelength), the absorption takes place closer to the surface. The absorption coefficient for Si rises slowly with decreased wavelength compared with the other materials shown in the diagram due to the indirect band gap.

2.5 The Band Gap

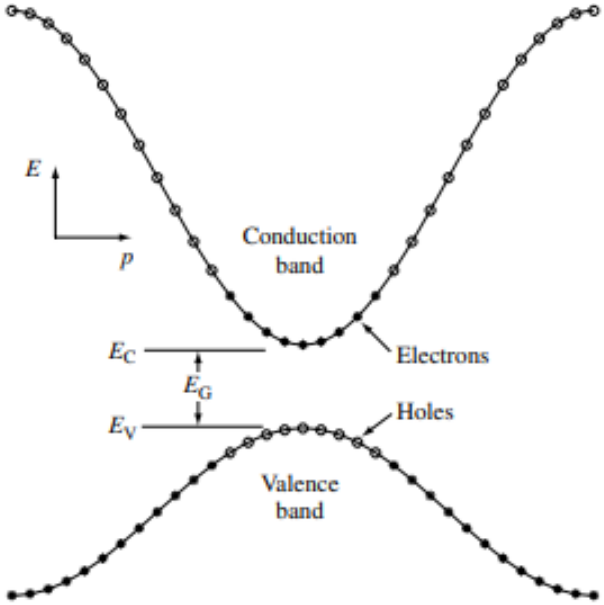

Figure 2.7: Simplified energy band diagram for direct band gap materials at T>0 K [8]

Both, the Fermi Energy level curves for the valence band and the conduction band have parabolic shapes in the crystal momentum or quasimomentum axis. When the minimum of the conduction band occurs at the same value of the crystal momentum as the maximum of the valence band, as it does in figure 2.7, the semiconductor is said to be a direct band gap semiconductor. When they do not align, the semiconductor is said to be an indirect band gap semiconductor.

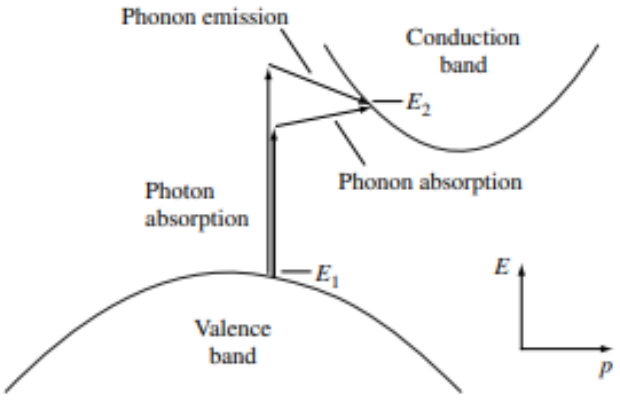

Figure 2.8: Simplified energy band diagram for Indirect band gap materials at T>0 K. Energy and Momentum are conserved by the absorption or emission of phonons [8]

Si and Ge are both considered indirect band gap semiconductors. In these semiconductors, due to the conservation of electron momentum, the photon

absorption must be facilitated by a phonon. A phonon is the particle representation of lattice vibrations in the crystalline structure. They are low-energy particles with relatively high momentum. This is illustrated in figure .

Since both, a phonon and an electron are needed to make the indirect gap absorption process possible, not only does the absorption coefficient depend on the concentration of initial electrons states and empty final states, but also on the availability of phonons (both emitted and absorbed) with the required momentum. Nevertheless, a direct transition without phonon assistance is possible in indirect band gap materials, as long as the photon energy is high enough, for which Si requires about 1.1 eV. Conversely, in direct band gap materials, phonon-assisted absorption is also a possibility, which may improve or deteriorate the ease at which the electrons transit to different energy bands. Compared to semiconductors with direct energy band transitions, the absorption coefficient for indirect transitions is relatively smaller. As a result, light penetrates more deeply into indirect band gap semiconductors than direct band gap semiconductors. The photons interact with fewer available electrons, which translates into thicker solar cells due to a greater absorption length.

2.6 Recombination

When a semiconductor is not in thermal equilibrium, for example by heating up the crystal lattice (by absorbing light that doesn't get used up in the photoconversion process, or for example through the ambient temperature), or by injecting current, or absorption of thermal lattice vibrations (phonons), they have a tendency to release this energy. The energy released can be in the form of photons or phonons [8]. This loss process is known as recombination, in which an electron falls from the conduction band to the valence band. It essentially depends on the concentration of electrons and holes. It aims to eliminate a valence band hole and restore the equilibrium concentration values for these chargers. There are mainly three recombination mechanisms important to the operation of solar cells. Recombination through traps (defects) in the forbidden gap, radiative (band-to-band) recombination, and Auger recombination. Recombination losses affect both the short-circuit current as well as the forward bias injection current (and therefore the open-circuit voltage). Typically, recombination at the surface or in the bulk of the solar cell are the main areas of recombination. The depletion region is another area in which recombination can occur. A good material with high chemical purity and structural perfection is required to fight the natural tendency of the conduction-band electrons to return to the valence band. To avoid this loss, the electrons must be highly mobile, as they are in perfect silicon. Impurities like dopants and imperfections further scatter the electrons, giving the holes and electrons a greater opportunity to recombine and release the energy in the form of heat, immediately restoring them to the valence band energy and reducing the concentration of free electrons travelling through the circuit.

2.6.1 Radiative (Band-to-Band) Recombination

Radiative recombination dominates in direct bandgap semiconductors. In indirect bandgap semiconductor, radiative recombination is extremely low and usually neglected. Essentially, an electron from the conduction band combines with a hole in the valence band and gives off energy as a photon. The emitted photon has an energy close to the band gap and has therefore a low probability of being absorbed, freeing itself [7].

2.6.2 Recombination Through Defect Levels

Also known as Shockley-Read-Hall (SRH) recombination, it occurs via a defect energy level in the band gap, introduced through intentional or unintentional defects in the crystal lattice as in doping. An electron or hole may move to an extra energy state in the forbidden region. If the opposing charge carrier moves up to the same energy state, then it recombines. The rate at which a carrier moves into the energy level in the forbidden gap depends on the distance of the introduced energy level from either of the band edges. Therefore, if an energy is introduced close to either band edge, recombination is less likely as the electron is likely to be re-emitted to the band rather than recombine with the opposing charge carrier [7].

2.6.3 Auger Recombination

In silicon based solar cells, auger recombination limits the lifespan and ultimate efficiency. Auger recombination happens when an electron and a hole recombine, but the emitting energy is absorbed by a third carrier, an electron in the conduction band. This electron then releases energy in the form of heat or a phonon and transfers back down to the conduction band edge. Auger recombination is most important at high carrier concentrations caused by heavy doping or in concentrated sunlight [7].

2.7 The breakdown effect

The breakdown behaviour is of paramount importance for the design of modern solar modules. A solar cell, when it is fully shaded within a module string, becomes reverse biased. Generally, in these situations, the current isn't homogeneously distributed throughout the cell area and tends to concentrate in small regions where the silicon presents a higher concentration of defects/impurities with slightly higher conductivity. If such a power dissipation is high enough, it produces a considerable temperature increase in the small regions close to impurity centres, thus giving rise to hot-spot heating. Under hot-spot heating, the temperature of the heated regions can exceed the maximum value tolerated by the PV cell, with possible consequent permanent

damage to the cell. Most of the breakdown spots on a solar cell can be classified according to the three different types termed types I, II, and III, and refers to how the current is continuously increasing with the reverse voltage. Type I (early) breakdown is characterised by a linear or only slightly superlinear characteristic, type II (defect-induced) by an exponential characteristic curve with medium slope, and type III (avalanche) with the steepest current increase of the three. The I-V characteristic curve for the diode at the reverse bias region is illustrated in figure 2.9.

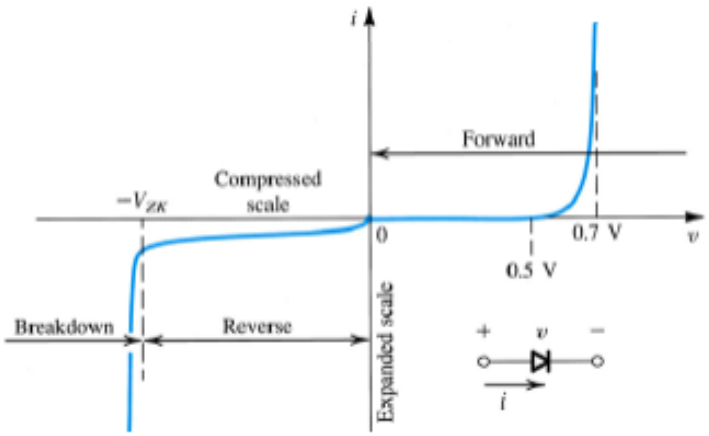

Figure 2.9: I-V characteristical curve for a typical diode [9]

To model the breakdown effect on a solar cell, literature often uses the Bishop model which proposes to add a parallel current to the shunt branch model where the breakdown effect is expressed as a non-linear multiplication factor that affects the shunt resistance (R_{sh}) current term [25]. A low value of Rsh originates a large photovoltaic current when the cell is reverse biassed, which in turn will produce a high power dissipation on Rsh [26]. A stronger ohmic shunt should prevent the formation of local high electric fields that are responsible for light emission. Modelling the breakdown phenomena will not be considered in the present work, however it is an issue of concern since this phenomena is required to assess the longevity, the temperature and other operating conditions of solar cells in the case of partial or full shading.

Chapter 3
Literature Review

First, the behaviour of the solar cells and panels are analysed when subjected to shade. Then, different kind of inverter topologies are discussed. Different mitigations tecnhiques are presented in order to mitigate the effects of shading.

3.1 Shading on PV modules

A PV module is highly dependent on the intensity of the solar irradiation incident upon it. The shading on PV panels, for instance, due to a passing cloud or neighbouring structure causes not only energy loss in the conversion, but also further non-linearity on the I-V characteristics. A shaded panel in a non-uniform illuminated PV system may display a negative voltage.

The existence of shaded cells, either partial or fully, in a module causes a mismatch on the equilibrium of photo-generation of electron-hole pairs of the cells [25]. Crystalline silicon solar cells in modules are connected in series and therefore carry the same current. However due to the different irradiation and current mismatch, a non-shaded cell of the module operates at a generation of carriers higher than those of the shaded ones [25]. Consequently, the shaded cells may be operating in the reverse bias mode. If there is no protection, the shadowed cells may begin to operate in the breakdown region. The shaded cells dissipate power in the form of heat in local hot spots, caused by a high bias voltage and breakdown event [27]. The increase in the power density and high local temperatures can damage modules, by damaging the solar cell, or the structure, and lead to failure of the soldering material, the glass and possibly melting the back sheet of the module [26]. The dissipation in the shaded cells can be limited with the use of bypass diodes connected in parallel with a subsection of the panel or with a full panel is common practice as a compromise between protection and increase in cost[28]. When the cell is shaded, the bypass diode limits the reverse voltage that can be applied to a cell, preventing it from reaching the breakdown voltage. A cell in reverse bias renders useless the rest of the cells under the bypass diode.

As mentioned above, the shaded panel of a non-uniform illuminated PV system can be submitted to a negative voltage. If there is no protection,

the shadowed cells may begin to operate in the breakdown region during non-uniform illumination. Some cells display a great reverse current before reaching the breakdown voltage which is due to impurities and defects that are commonly modelled by a shunt resistance, whose value depends on the distribution and concentration of impurities inside the cell [3]. If the shunt resistance is too low the hot-spot condition can occur before the PV cell enters the breakdown voltage even if bypass diodes are used, once again, allowing the PV cell to reach a high enough temperature and cause permanent damage. *Bende, EE et al.* [26] demonstrated that although low shunt resistance cells do dissipate more power at higher shadow fractions, this wasn't the case for cells with high shunt resistance. These cells showed a maximum dissipation at shadow fractions between 5% and 18% under nominal MPP and optimised MPP conditions, respectively [26]. *Wohlgemuth, John et al.* [29] returned results similarly between 12% and 15%. Solar cells with low shunt resistances showed a maximum power dissipation level at high shading fractions. For solar cells with high shunt resistances and high breakdown voltage, the power dissipation in the shaded cell was only proportional to the produced photon current up to the maximum dissipation point. While for cells with high shunt resistance and a low breakdown voltage, the power dissipation was lower [26]. In a study conducted by *Geisemeyer, I et al.2014* [30], the maximum power dissipation in multi-crystalline silicon cells ranged from 60-90 W from the MPP to short-circuit conditions respectively. Therefore, in industry, many manufacturers measure the reverse I-V characteristics of produced cells and apply a rejection criterion, typically of 2.5 A, at a reverse bias of -10 V [26]. This is suggested to be sufficient to prevent hot spot failures in modules with fully shaded cells [31].

Teo, JC et al.2008[32] found that when 20% of photovoltaic modules in the photovoltaic system were shaded by an identical shading configuration, the maximum power dropped by approximately 6.22% for every 100 w/m^2 drop between 1000 and 700 W/m^2 [26]. However, when the shaded modules irradiance dropped below 700 W/m^2, the maximum power lost was only 0.24% for every 100 W/m^2 drop in the shaded module irradiance. This means that the photovoltaic system becomes resistant to shading heaviness as the shaded modules irradiance reaches a critical point [32]. If the critical point is known, some unnecessary reconfiguration switching can be reduced as the photovoltaic system becomes resistant to shading heaviness when the critical point is met

Anjos et al.2017 [33] and in *Giaffreda, Daniele et al.2011* [25] both analyse the evolution of the temperature in a silicon crystalline PV module under hot spotting conditions and concluded that partially shaded PV cells suffer from hot-spots at a faster rate than a fully shaded cell. This is theorized to be due to part of the cell still being fully irradiated, while also under the effect of the reverse bias, leading to a higher operating temperature[25]. Therefore half-cut cells could be preferred to larger cells [25].

Dolara et al.2013 [28] conducted experiments recording the current–voltage, and calculated the power–voltage characteristics of various modules, operat-

ing at different conditions. Both, the vertical and horizontal shading pattern effects on PV modules and output power reduction were analysed. The paper in conclusion emphasises the importance the role of bypass diodes in the PV modules. These diodes divide each module into several sections, limiting the production's decrease caused by the shading conditions. For a single cell, as the shading profile is varied between 0% and 100%, the generated current decreases accordingly [28]. As the shading profile increases, the maximum power production decreases critically when the shading profile reaches 50% of the cell. Beyond 50% shading, the MPP's begin to be located very far from the normal MPP region and start depending only on the two unshaded sections of the PV module [28].

For a PV module, by increasing the shading profile vertically on the module between non shaded and fully shaded (0% and 100%) determines similar results as the ones obtained by shading a single cell. Because the cells vertically have a series connection, by shading one cell or shading a column of 10 series-connected cells determine the same result, the current flows through the by-pass [28]. Similarly, shading a line of cells or shading two lines of cells vertically, composing a module's sub-section, leads to the same result. In the horizontal configuration, by increasing the shading profile in the horizontal influences all the three module's subsections. In this case, the generated current critically decreases until it becomes zero when an entire horizontal line of cells is shaded. This means all three subsections have at least one cell that is fully shaded. For a diagonal shading pattern, a mixture of both effects take place. The current produced depends on if a cell is totally shaded and which sub-sections are under the effect of the shade. There is a decrease of the generated current as the shading profile is increased. The electrical current generated by the shaded subsection of the module becomes zero when a cell becomes completely shaded. These findings are rather important when designing a photovoltaic system due to the shadow effect of an adjacent panel, which may be overlapping with the module. Appropriate calculations of the tilt and necessary distances between rows or columns for a given location and relative position with the sun during peak production hours are therefore an important aspect to be considered while designing a PV system. The study concludes that the effect of a hard shadow on a module's power generation by shading a single-cell is not dependent in a critical manner on the shading profile (right-to-left and bottom-to-top), or on the poly-crystalline or mono-crystalline typology. However, when scaled up and analysing the module's power production, the power production it was very much dependent on the shading profile.

Abdullah, Ghoname et al.2021 [34] investigate experimentally on the power output affected by partial shading conditions (PSCs) in a photovoltaic array with a series configuration. As the amount of shade increased, the value of the fill factor decreased. The fill factor was high when the PV array performance was higher. The results showed that 44% shading of the first PV cells affected the PV array power output loss by more than 80%. For the case

of a series configuration, it was seen that even if only one PV module fails to generate electricity due to the event of failure, the total amount of power generation of the whole PV array is reduced.

In a study by *Guo, Siyu et al.2012* [22], a PV module with 60 cells (six cells in width and ten cells in length), was investigated in terms of performance under different shadow transmittance. The shadow moved one PV cell length during every half-hour period and took three hours to reach the last cell's end when the shadow moved horizontally. They found that the shadow on the PV module's second cell caused more power output loss compared to the first solar cell.

Ahmad, R et al.2017 [27] suggests that partial shading (PS) is a frequent phenomena where some modules within an array receive different levels of irradiance. Since the short-circuit current of a PV module is proportional to the irradiance level, the modules under PS start producing less current, while the un-shaded modules continue to operate at a higher photocurrent. As the string current must be equal through all the series-connected modules, the shaded modules as a result, similarly to the cells, operate in the reverse bias region to support the common string current [27]. In their paper each PV module contains a single by-pass diode. As the shaded modules begins to operate with reverse voltage polarity, they begin to consume power, reducing the maximum extractable power from the shaded PV array. The bypass diode becomes activated as the reverse voltage across the shaded module increases. Since the bypass diodes provide an additional current path, modules of a string no longer carry the same current when partially shaded and the common string current flows through the bypass diode instead. Therefore, the P-V curve develops multiple local maximums, (LM), which occur at integral multiples of the open circuit voltage of the module (Voc) [27]. These voltage points are known as Inflection Points. This paper suggests that the maximum number of LM's in a PV array doesn't exceed the number of series connected modules under any kind of partial shading configuration. In each zone between two integers of Voc, even if the local maximum are different in the strings connected in parallel, the resulting LM in the PV array is only one. This paper also provides information on the behaviour of the local maximums in terms of the Voc and the short circuit current (Isc) based on the position for a bottom corner triangular shading pattern of the panel.

3.2 Grid Connection

Hassaine, L et al.2014 [35] gives an overview of power inverter topologies and control structures for grid connected photovoltaic systems. In PV systems connected to the grid, the inverter, which converts the output direct current (DC) of the solar modules to the alternate current (AC), has generated some research interest. There are essentially four different ways to convert the current. There are centralised inverters, multi-string inverters, string inverters and

module-based inverters or micro-inverter configurations. The configuration of the PV panels and proper selection of the inverter will directly have an influence on the cost and efficiency of the entire system [35]. The choice is largely dictated by the power requirements of the system [35]. Centralised inverters are based on the connection of a large number of PV modules to an inverter, mostly used in medium and high power PV system applications, (power levels of 10–250 kW) [35]. The most crucial drawback of these inverters is mismatching losses. Different orientation of modules and different shading conditions, compromises the whole system. There are different configurations that can be established between the panels and different reconfigurations systems which can be employed to mitigate these problems, [36],[37], however, without these techniques, these inverters suffer from missing individual MPPT, losses in the string diodes and losses due to the high-voltage DC-cables between the PV modules and the converter. The popularity of the central inverter is mainly due to it having a high efficiency and low cost. However, the non-flexible design make it unsuitable for mass production. The grid-connected stage is usually line commutated by means of thyristors, involving many current harmonics and poor power quality [35]. The failure of the central inverter results in that the whole PV plant fails to operate.

String inverters can be considered as a reduced version of centralised inverters [38][35]. The input voltage may be high enough to avoid voltage amplification [35]. This type of inverter is usable for mismatch applications because each string is attached to one inverter and thus the orientation problems are reduced. There are no losses associated with string diodes and individual MPPT of each string is viable. Consequently, this configuration increases the overall system efficiency when compared to the central inverter. However, it remains in disadvantage when compared to the latter as the rather low power level per inverter, leads to a higher price per kW [38]. Though it should be mentioned these inverters have the ability to be mass produced, which lowers their initial cost and have evolved as a standard in PV system technology for grid connected PV plants [35].

The Multi-string inverter is a variation of the string inverter with an extra input. Several strings are interfaced with their own DC–DC converter (separate MPPT systems) to a common DC–AC inverter. The multi-string inverter configuration, although formed on more than one distinct and independent PV panel string, each string has its own MPPT connected to a unique inverter[38]. Multi-string inverters allow for different orientations. Moreover, it can reach a higher power level than a string inverter and removes the higher price per kWh [38]. When designing a plant, fewer components are needed when compared to string converter. This benefits the cost and lowers the labour needed. Because of having multi-stage designs, the input voltage has a wider range. Hence, it may benefit from the daylight and its fluctuations more than other types of inverters, increasing power generation capabilities[38]. This is beneficial, compared to the centralized system, since every string can be controlled individually. Accordingly, a compact and cost-effective solution, which combines

the advantages of central and string technologies, is achieved [35], [38].

Micro-inverters (MIs) have been becoming more popular within the field of photovoltaics, gaining more traction on the market. They offer several advantages such as low converter power rating and low power losses, while accurately tracking the maximum power point in partially shading conditions and eliminating mismatches in a system while helping increase its reliability. MIs are mostly designed for power rating between 50 and 400 W with power conversion efficiencies above 90% [38]. There are modules which incorporate an MI by design, these are known as AC modules. The design power output for the AC module is typically around 100 W [38]. However, the low power level for MIs may reduce the overall efficiency. The necessary high voltage-amplification may also reduce the overall efficiency and increase the price per watt because of more complex circuit topologies[38]. These kinds of inverters remove the bulk of DC cabling, and it includes the possibility of a facilitated enlargement of the system, due to the modular structure. These systems come with a few disadvantages, the number of parts significantly increases as does the increase in costs and workmanship, which can be a turn-off as each panel is equipped with its own MI [38]. Furthermore, the inequality between inverter lifetime and panel lifetime is another handicap which deters the use of these systems [38].

A single central inverter or multiple string inverters will be chosen, depending on the designer and the needs of the system. Technically it is possible to use both topologies [35]. Therefore, for large-scale solar power generation it is necessary to optimise the topologies and the PV system design to make solar energy economically acceptable and attractive. There are many aspects to evaluate a PV system design, such as efficiency, reliability, cost, energy yield and lifetime capabilities [35]. The need for these different kinds of setups will depend greatly on the irradiation and shadowing conditions to which the panels will be subjected.

3.3 Optimisation

Madhukumar, Mithun et al.2020[39] presents a comparative analysis of both the perturb-and-observe and incremental conductance MPPT techniques using a boost converter implemented in Matlab/Simulink 2020 to track the performance of both these MPPT methods. Maximum power point tracking controllers are important when environmental changes and varying irradiance patterns are affecting the PV system as these controllers help extract the maximum power from PV modules and assist with reaching that point[39]. *Ali, Amjad et al. 2020*[15] present an overview and classify different MPPT algorithms under both uniform and non-uniform irradiance conditions. It summarizes various methods by analysing their mathematical expression, operating principle, and block flow charts.

The hardware implementation of these solutions is not always easy and

when a bug occurs, it is difficult to know exactly the responsible component of this bug (PV panel, DC/DC converter, sensors, actuators and microcontroller) and so this process takes longer [15].

Nguyen[40] wrote a PhD thesis regarding the modelling and reconfiguration of solar photovoltaic arrays for non-uniform shadow conditions. In utility grid connected PV systems, the fast reduction in supply power can cause instability to the whole system. This thesis models and simulates through a computing algorithm the effect of non-uniform changing shadows to be used in real time controllers.

PV array Reconfiguration strategies used to increase maximum power output under partial shading conditions by changing the panel connection in an array or from one array to another. *Krishna, G. et al. 20197* [37] in their paper address the topic of reconfiguration strategies which can broadly be classified into dynamic PV array reconfiguration techniques (DPVAR) and static PV array reconfiguration techniques (SPVAR). The dynamic technique is an alternative to distributed MPPT techniques for mismatch phenomenon. DPVAR systems require suitable measurement devices for the both physical and electrical parameters as data for the acquisition system and the validation of the mathematical model. The algorithm quantifies the unknown parameters, which in turn, by identifying the optimum configuration, sends a control signal to the switching matrix [37]. If one module begins to fail, it can quickly be identified and automatically disconnected. Static techniques on the other hand are based on the dispersion of shade by physically relocating shaded panels to the unshaded positions to equalize the row current. In SPVAR, the PV modules are rearranged within the in such a way that the irradiance is equally spread. The main drawback is it cannot self-reconfigure. Another drawback is that in all arrangement schemes, if the shadow falls on the first column of the array, the power isn't distributed, which reduces the amount of power extracted by the array. this technique may also fail to distribute the shading effects in cases envolving mutual shadow and fast-moving clouds, [37].

Pachauri, Kumar et al. 2020[36] presents a comprehensive review of various PV array configuration models and approaches for shade mitigation under partial shading conditions. Different PV array configurations are reviewed and considered in terms of their accuracy and reliability, location of the global max power, qualitative performance parameters such as efficiency and the Fill Factor, along with hardware implementation and complexity. The strengths and weaknesses of each scheme are pointed out. These PV array configurations are categorized as conventional, reconfigured, puzzle-based configurations and meta-heuristic algorithm switching configurations [36]. Within the conventional configuration category, the Total Cross Tied (TCT) scheme was found to have the best relative performance. They also explore puzzle based configurations and compare them to conventional configurations showing the puzzle based configurations to be an improvement. Meta-heuristic algorithms such as particle swarm optimisation and social mimic optimisation are discussed and concluded to be an even greater improvement on puzzle based schemes [36].

The Master's dissertation in ref [41], studies the effect shade has on multi crystalline silicon cells. In the case of a string of six modules, it is shown that installing an optimizer does not increase the output when they all are under the same shade configuration or are unshaded. They do however, increase the power of module if all three circuits in the module are partially shaded. Optimisers were seen beneficial to install when the module has one bypass circuit shaded less than 50% or two bypass circuits shaded less than 80%, leaving the max power point of the module is in the lower step of the I-V curve [41].

Bende, EE et al.2014 [26] concludes that by optimising power at a module level would improve the performance and safety of the module compared to a system level approach in partial shading conditions. Global MPP trackers in central inverters have the advantage of determining the MPP, however they may pose a safety and long-term reliability issue as to achieve the MPP, the shaded solar cells begin to work in reverse bias and dissipate power in the form of heat [26].

Dekker, NJJ et al.2020 [42] suggests employing power optimisers in a cost-effective manner by using them in modules that are susceptible to partial shading conditions, however cautions about the need to understand the shadow configuration in order to properly ascertain under what circumstances they should be used. It concludes that the use of power optimisers on the shaded module, for a limited shade (10%-40%), on a single cell prevents the occurrence of hotspots and therefore improves the lifetime of the module, but no significant change was observed in the extracted power. The employment of these systems on multiple cells and substrings of a module, do significantly improve the power output and are advised. If a shade of 10%-40% occurs on multiple cells and substrings of a module, optimizers do significantly improve the amount of power extracted [42]. By applying a shade of 40% covering a 1/3 of the total number of PV modules, the expected gain by power optimisers is 30% [42]. When the module is subjected to higher shade percentages (above 40 %) covering several cells in the substring, power optimisers don't contribute meaninfully as the power no longer concentrates over one cell and dissipates over the shaded cells and no extreme temperatures occur [42]. In conclusion, power optimisers are advised for a higher power output, however their relevance becomes less significant as the amount of shade and modules shaded increases.

Newman, BK et al.2019 [43] studied the effect of dynamic shading on multi-crystalline Silicone modules equipped with power optimisers by measuring its response. They did not find a difference in the power in the case of partial dynamic shade that is parallel or perpendicular to the strings. In both cases, the module level power optimiser remained around the local maximum power point and did not complete a global sweep, which only took place every few minutes. Most significantly, they compared two commercial optimisers, a fast optimiser and a slow optimiser, under a single fast shade, lasting approximately 0.45 seconds, and observed their power recovery. The slow optimizer recovered about 100 milliseconds faster to the initial state than the fast opti-

mizer, which performs a maximum power point sweep in a shorter amount of time. The voltage signal for the slow optimiser found no significant changes while the voltage of the fast optimizer was amplified trying to find a local maximum [43]. In quick moving shade, due to the MPP always changing, the slow optimizer hasn't performed a sweep and therefore is less sensitive to the disturbance and recovers more readily without any over-correction [43].

Ramli, Makbul AM et al.2017 [44], focus on the potential of solar and wind energy-based distributed generation (DG), with the aim of maximizing the available resources in various regions of Saudi Arabia. They present the progress of DG applications in terms of research, planning, and exploitation of wind and solar energy resources, assessing the contribution to the energy sector of Saudi Arabia. They also emphasise some of the major challenges, including the high temperatures of the region and the dust on the panels which may result in partial shading, affecting power output and the overall performance the system. Tracking the MPPT, and automatically adjusting the control algorithms of the power electronic devices during time of variations of; light level, shading, temperature, and PV characteristics, is suggested as a solution. However, the authors believe that the investment brought about the increase cost of equipping PV systems with embedded MPPT algorithms, need to be carefully considered to not deter possible investors.

3.4 Visualization and quantitive analysis

The problem of dynamic shading due to wind turbine blades represents a complex problem to solve. Recently, several software solutions with the use of powerful graphics processing units have been developed to satisfactorily solve complex shading patterns and offer a meaningful way forward in modeling and analysing the dynamic shading problem [45]. In the present work, this approach isn't possible as the resources available do not permit it. Instead the shading is simplified and assumed to completely cover the irradiation and endure for 0.5 second intervals. In reality the time the shade lasts and the total period of the shading event depends on the area covered and the speed at which the blades of the turbine rotate.

Chapter 4

Mathematical Modeling of a PV cell and module

4.1 The 5 Parameter Model

A photovoltaic cell is usually a semiconductor device that converts sunlight into electricity by the means of photovoltaic effect. Predicting the behavior of I-V and P-V curves for photovoltaic (PV) generation is possible through mathematical models for photovoltaic cells. Several models for silicon photovoltaic cells are proposed in literature [34], [46] and [47]. Among these, the single diode model offers a good compromise between simplicity and accuracy, being widely used for this reason. This model of a PV cell is shown under the equivalent circuit in figure 4.1.

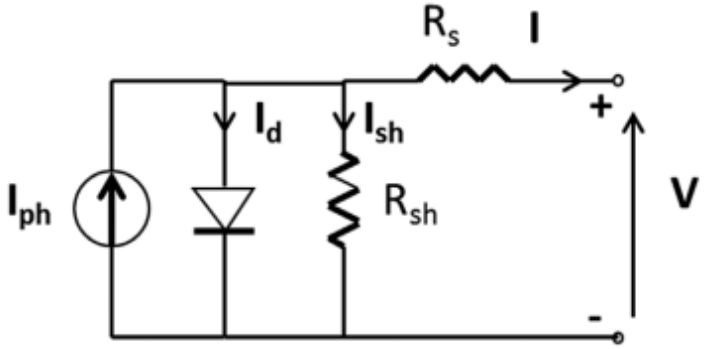

Figure 4.1: Equivalent 5 parameter electrical circuit [10]

For PV cells the equivalent 5 parameter circuit consists of a current source, a diode, a series resistance and a shunt resistance. The five parameters that need extracting are the incident photon current I_{PH}, the saturation current I_O, the series resistance R_S, the parallel resistance R_{SH} and the ideality factor of the diode n. The precise modelling of a solar cell is based on the accuracy of the extracted parameters of that model. The output current of the cell can be determined by the equivalent circuit expressed in equation 4.1.

$$I = I_{PH} - I_0 \left(\exp \frac{q(V + I \times R_S)}{n k_b T} - 1 \right) - \left(\frac{V + I \times R_S}{R_{SH}} \right) \tag{4.1}$$

Here, q is charge of electron, k_b is the Boltzmann constant, T is the cell operating temperature and V is the cell output voltage. The photocurrent I_{PH} which is a function of cell operating temperature and solar irradiance is expressed in equation 4.2. The diode term, represented by the second term of equation 4.1,models the inherent dark current I_d, formed by the nature of the p-n junction, equation 4.2. Essentially The diode term determines the I-V characteristics of the solar cell per the Shockley equation and the combination of the first two terms are sufficient to map the I-V characteristic of the load, figure 4.2. The final term of equation 4.1 represents the shunt current Ish, attributing to the parasitic current which models the noise current between the top and the bottom of the solar cell.

$$I_{PH} = I_{sc} + K_I \left(T - 25 \right) \frac{G}{1000} \tag{4.2}$$

I_{sc} represents the short circuit current at reference temperature and irradiance, while K_I is cell's short circuit current temperature coefficient, which models a linear dependency with the temperature, and $G/1000$ represents the relationship between the solar insulation and the reference conditions which is 1000 W/m^2.

$$I_d = I_0 \left(\exp \left(\frac{q(V + IR_s)}{n k_b T} \right) - 1 \right) \tag{4.3}$$

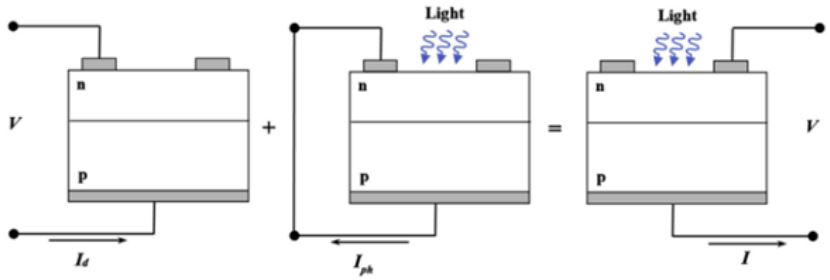

Figure 4.2: Visual representation of the essential contributing parameters for mapping the I-V characteristic load represented in equation 4.1, from ref[3].

$$I_0 = I_{rs} \left(\frac{T^3}{T_{ref}} \right) \exp \left(\left(\frac{qE_g}{n k_b T} \right) \left(\frac{1}{T} - \frac{1}{T_{ref}} \right) \right) \tag{4.4}$$

From equation 4.3, the term for the saturation I_0 can be expanded as equation 4.4, which follows a cubic relationship with the operating temperature. Here, I_{rs} is the reverse saturation current and E_g represents the band

gap of the material which is approximately 1.1 eV for silicon. I_{rs} at reference temperature can be approximately obtained as, equation 4.5.

$$I_{rs} = \frac{I_{sc}}{\exp \frac{qE_g}{nk_bT} - 1} \tag{4.5}$$

Finally, depending on the amount of connected in series cells, N_s, The Voltage of the Pv module V_m can then be obtained by equation 4.6 .

$$V_m = N_s \times V \tag{4.6}$$

4.1.1 Qualitative parameters

The behaviour of solar cells and modules can be measured using qualitative parameters such as the fill factor and the efficiency, both of which are highly dependent on the short circuit voltage Voc and open circuit current Isc. The fill factor (FF) is a parameter which, in conjunction with Voc and Isc, determines the maximum power from a solar cell.

$$FF = \frac{P_{MP}}{V_{OC} \times I_{SC}} \tag{4.7}$$

It essentially measures the position of the maximum point of power generation, that is the product of Vmp and Imp relative to the open circuit voltage and short circuit current, that is, the squareness of the I –V characteristic curve. It gives information about the quality of the solar cell and is always less than one.

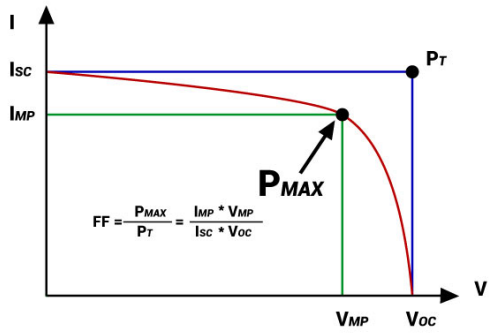

Figure 4.3: Definition of Fill Factor in the I-V curve [11].

The efficiency on the other hand measures the ratio of Power of the incoming photon flux with the maximum output power of the solar cell.

$$\eta = \frac{V_{OC} I_{SC} FF}{P_{in}} \tag{4.8}$$

The light intensity has an impact on all the parameters of the solar cell. Both the short-circuit current and the open-circuit voltage increase with an increase in light intensity, as do both the series and shunt resistances.

4.1.2 I-V Characteristics of Junction Diodes

The current-voltage (I-V) characteristics of a junction diode depend on the diode saturation current, the ideality factor and the thermal voltage,V_t , equation 4.9. As can be seen in figure 4.4, the diode I-V characteristics takes on an exponential form.

$$V_t = \frac{q}{nKT} \tag{4.9}$$

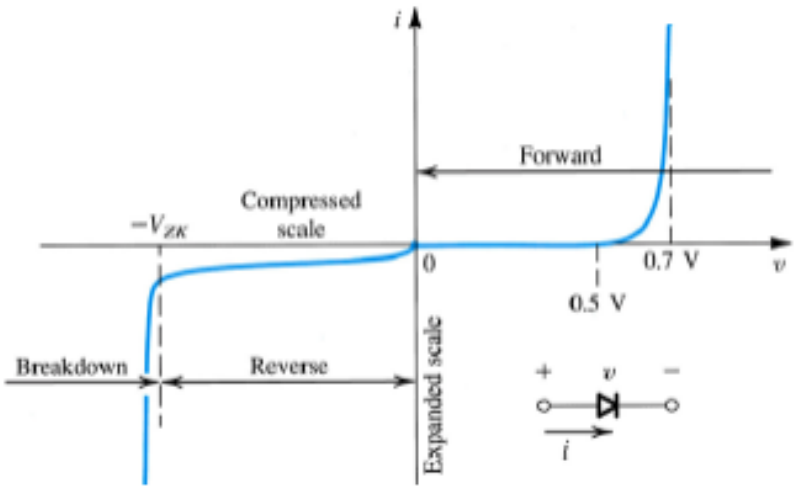

Figure 4.4: I-V characteristic of a diode

4.1.3 Effect of series resistance

The effect of the series resistance can be seen near the short-circuit conditions in figure 4.5, and through the deterioration of the slope of the I-V curve at the open circuit voltage. The open-circuit voltage isn't affected by this parameter since the overall current flow through the solar cell is null. The main impact of this parameter is the reduction of the fill factor, although excessively high values may also reduce the short-circuit current. The major contributors to the series resistance are the movement of current through the emitter and base of the solar cell, the contact resistance between the metal contact and the silicon, and finally the resistance of the top and rear metal contacts.

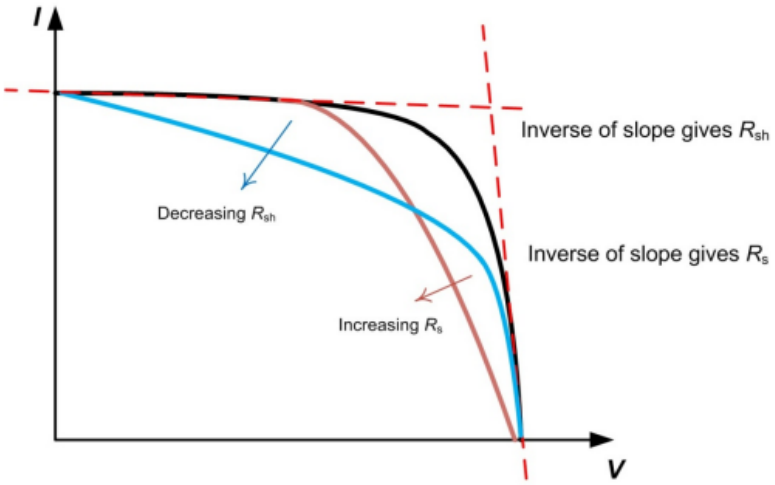

Figure 4.5: Effect of altering either the series resistance or the shunt resistance in the I-V characteristic curve [12]

4.1.4 Effect of shunt resistance

The effect of the shunt resistance can clearly be seen near the open circuit voltage, figure 4.5, and through the alteration of the slope of the I-V curve at short circuit conditions. The shunt resistance appears in parallel with the series combination of series resistance and load resistance. As the shunt resistance is reduced the voltage across it and the parallel diode in the solar cell model decreases. This causes reduction in the output voltage across the load. Shunt resistance typically increases near the edges of the cell due to partial shorting in that area and may also be increased through manufacturing defects or doping.

4.1.5 Effect of Temperature

Solar cells in direct sunlight can be somewhat 20℃ – 30℃ warmer than the ambient air temperature. The efficiency of a solar cell depends on the cell temperature and is open to variation due to a variation of the ambient or operating temperature. Changes in insolation and in temperature causes variation to the response of the cell. The cell temperature is defined in equation (4.10), valid for a wind speed under 1 m/s. Here T_a represents the ambient temperature and $NOCT$ the nominal operating temperature given by the manufacturer [46].

$$T = 273 + T_a + \left(\frac{NOCT - 20}{0.8}\right)\frac{G}{1000} \tag{4.10}$$

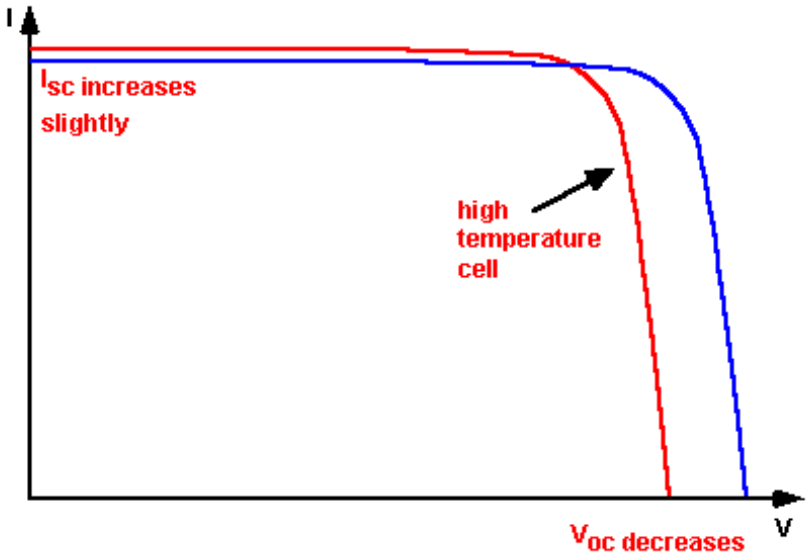

Figure 4.6: Effect of Temperature increase on the I-V characteristic curve [7]

As seen in figure 4.6, the temperature deteriorates the I-V curves by decreasing the open circuit voltage, although marginally increasing the short circuit current. The negative influence on the open circuit voltage is greater than the positive influence on the short circuit current.

4.1.6 Effect of Ideality factor:

The ideality factor of a diode is a measure of how closely the diode follows the ideal diode equation and is responsible for how the carriers interact. The value of the ideality factor varies in accordance with its characteristics. If the movement of the electrons is purely diffusive then the value of n is 1, where the recombination is limited by minority carriers. If recombination takes place in the depletion region then the value for n is approximately 2. At a value of 2 the recombination is limited by both carriers. In the range of 2 to 3, two majority carriers are necessary for every one minority carrier.

Chapter 5
DC converter

5.1 DC-DC Converters

Dc-dc converters are generally used to either step up or step down the dc input voltage. There are various converter topologies each with their own principle of operation, advantages and disadvantages. However, the buck and boost are the two basic converter topologies from which the other converters are derived from. A boost converter, figure 5.2, is used to step up unregulated dc voltage to the higher constant output voltage required by the load. The design and development of boost converter is mainly efficiency, output power and ease of design. This converter contains a switch, which is controlled by a PWM signal.

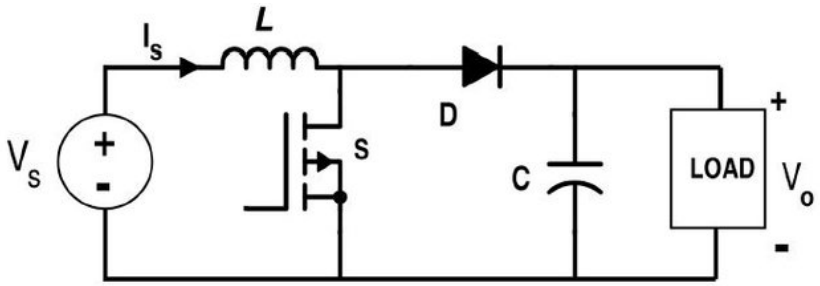

Figure 5.1: Electric circuit of a boost converter [10]

The process of energy absorption and injecting becomes a switching cycle in which the average output voltage depends on the duration of either states, as expressed by the duty cycle d. When the duty cycle d is on, the switch diode is turned on, which shorts the circuit. In return the conductor L stores energy and develops a greater difference in potential and it is the output capacitor that provides current to the load. When the cycle is turned off (1-d), the energy stored in inductor L is transferred to the load and its current falls until it is switched on again in the next cycle, as the forward bias diode connects the PV generator to the output. There are two different modes of conduction according to the behaviour of the inductor current. The two modes are continuous conduction and discontinuous conduction. Under discontinuous conduction,

there is an interval of time for which the current flow is zero, and no current is flowing from the inductor [13].

To dimension the converter to work in the continuous mode, we consider the methodologies presented in [10] [13] [48]. The switches are treated as being ideal, and the losses in the inductive and the capacitive elements are neglected. It should be mentioned however, that such losses can limit the operational capacity of some of these converters.

Under steady state and ideal conditions, without energy losses, the total energy which is saved by the inductor during the on switch of the cycle is the same as the amount transferred from the source to the output capacitor through the inductor during the off portion. Since in the time integral of the inductor voltage over one time period must be zero, yields the following equations.

$$\frac{V_0}{V_i} = \frac{1}{1-D} \tag{5.1}$$

$$\frac{I_0}{I_i} = 1 - D \tag{5.2}$$

The correct sizing of the duty cycle can now be obtained in terms of the panel output and the load, equation 5.3

$$D = 1 - \sqrt{\frac{R_{mp}}{R_0}} \tag{5.3}$$

To obtain the correct sizing of the inductor based on the current ripple, its value can be calculated by equation 5.4.

$$L = \frac{R_0}{\Delta i} \frac{D(1-D)^2}{f_{sw}} \tag{5.4}$$

Where Δi represents the inductor current ripple and f_{sw} the switching frequency. By specifying an acceptable current ripple value, the value of inductance can be determined.

The input capacitor can be designed based on equation 5.5 below, [10].

$$C_{in} \geq \frac{D}{8 \times f_{sw}^2 \times L \times 0.01} \tag{5.5}$$

And the minimum value of the output capacitor can be designed as equation 5.6 below, [10].

$$C_{out} \geq \frac{D}{f_{sw} \times 0.02 \times R} \tag{5.6}$$

Choosing values below the minimum indicated by these equations forces the converter to begin operating in the discontinuous mode.

To track the peak-to-peak ripple in the output voltage, it can be calculated by assuming that all the ripple current component of the diode current

flows through the capacitor and its average value flows through the load resistor. Therefore, the peak-peak voltage ripple is given by equation 5.7 (assuming a constant output current) [48].

$$\Delta V_0 = \frac{I_o D}{C f_{sw}} \tag{5.7}$$

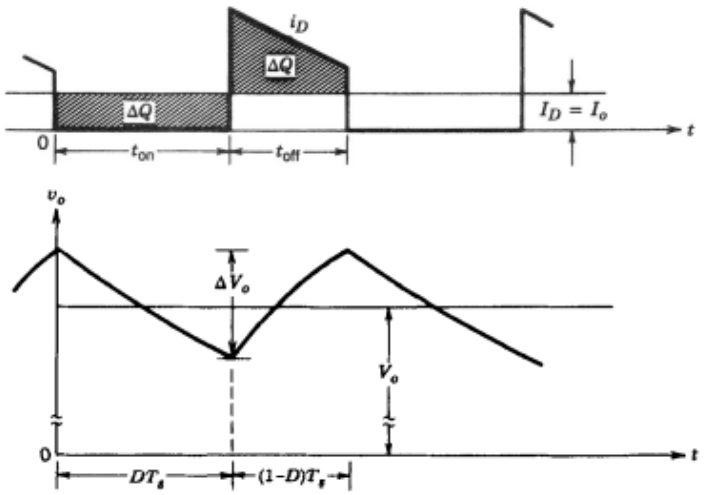

Figure 5.2: Voltage ripple [13]

5.2 Active Power Control

Active power control in PV systems can be achieved in several ways. *Sangwongwanich, Ariya et al.2017* [49] presents different relatively simple to implement strategies for active power control. The most commonly-used solution is to integrate the energy storage system to flexibly control the active power injection to the grid. However they are a bit expensive and offer a limited lifetime. Another way to achieve a flexible active power injection is by controlling the local load to absorb (e.g., smart loads) or dissipate (e.g., dump loads like resistors) according to the control. A more cost-effective way to realize the power control is by power curtailment. In this case, the Maximum Power Point Tracking (MPPT) algorithm is regulated, by comparing the output with a reference value or by a fitness algorithm. By doing so, the active power control doesn't require any extra components and is easily implemented as it requires minimum software modifications. Therefore, it is a cost-effective approach to realize flexible active power control in PV systems.

5.3 Max Power Point Tracking Algorithms

As the P-V characteristic is constantly varying by changing the irradiance and temperature, the MPP must be tracked to maximize the output power from the panel. The point at which I_{mp} and V_{mp} meet is the maximum power point. If the load line crosses this point, then the maximum power can be transferred to this load. The value of this load resistant can be given by:

$$R_{mp} = \frac{I_{mp}}{V_{mp}} \tag{5.8}$$

The different irradiation conditions make it necessary to determine an operating range, figure 5.3. If Ro is not within the optimum range, D of the boost converter becomes lower than the minimum duty cycle limit, Dmin, or higher than the maximum duty cycle limit, Dmax. If the duty cycle range is too small, the optimum point is not obtained and as a result, a variable output resistance should be considered.

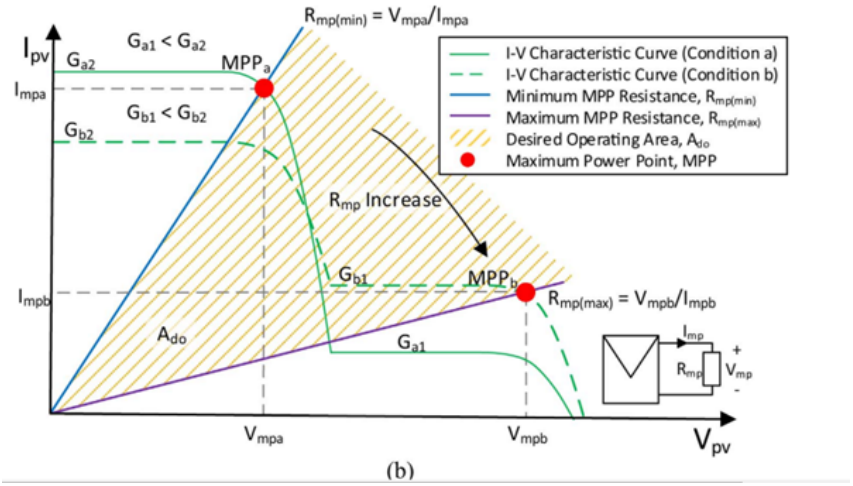

Figure 5.3: Representation of the operating area of the system under the I-V characteristic curve for different operating conditions [14]

In general, MPPT algorithms procure the optimum point of operation and outputs a duty cycle in order to control the switching cycle of the converter, achieving a better performance. There are different kinds of MMP algorithms and optimization techniques that can be employed. Ref [15] presents a useful overview of the different techniques.

5.3.1 Perturb and Observe Algorithm:

The Perturb and Observe ($P\&O$) is an iterative algorithm that compares the PV output power with that of the previous perturbation cycle. It's flow chart is illustrated in figure 5.4. When an increase in voltage leads to an increase in power, this means the operating point of the PV module is on the

Present perturbation (dV)	Change in power (dP)	Next perturbation direction
$dV > 0$	$dP > 0$	Positive
$dV > 0$	$dP < 0$	Negative
$dV < 0$	$dP > 0$	Negative
$dV < 0$	$dP < 0$	Positive

Table 5.1: Summary of the action of the Perturb and Observe algorithm [15]

left of the MPP. Hence further perturbation is required towards the right to reach MPP.

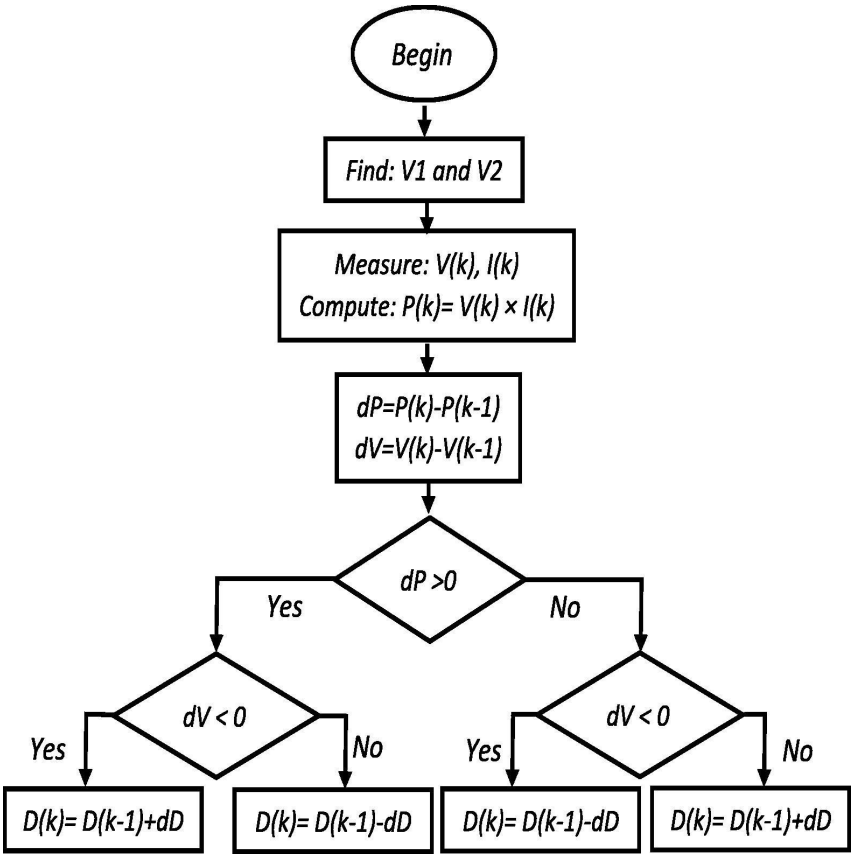

Figure 5.4: Perturb and Observe flowchart

Conversely, if an increase in voltage leads to a decrease in power, this means the operating point of the PV module is on the right of the MPP and hence further perturbation towards the left is required. The direction of the perturbation is summerized in table 5.1.

When the algorithm reaches a steady state, the power output oscillates around it's peak, which results in a small power loss, exacerbated by fast changing conditions. To keep the variation in power small, the size of the

perturbation is kept small. The greater the perturbation, the greater the power variation.

This algorithm has the disadvantage of failing to track the power under fast varying atmospheric conditions. Nevertheless, it is simple and widely accepted.

5.3.2 Incremental Conductance

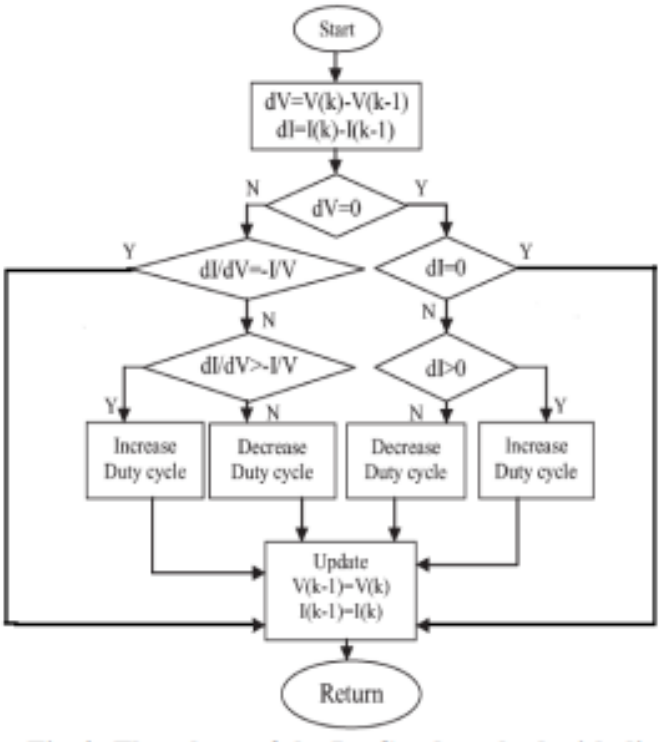

Figure 5.5: IC flowchart [15]

For the Incremental conductance algorithm (IC) the direction in which the MPPT operating point must be perturbed can be calculated using the relationship between dI/dV and $-I/V$, which is derived from the fact that dP/dV is negative when the MPPT is to the right of the MPP and positive when it is to the left of the MPP. If the value of incremental conductance is equal to that of instantaneous one, it means that the maximum power point is reached. The control action can be summerized by table 5.2.

The IC has the advantage of determining the MPP under quickly varying irradiance conditions with higher accuracy. However it is a bit more complex. This method exploits the assumption that the ratio of change in output conductance is equal to the negative output instantaneous conductance.

Mode	Perturbation		MPP Level	Status
Mode-1	$\frac{dP}{dV} = 0$	$\frac{\Delta I}{\Delta V} = -\frac{I}{V}$	At MPP	Hold $V_{PV} = V_M P_M$
Mode-2	$\frac{dP}{dV} > 0$	$\frac{\Delta I}{\Delta V} > -\frac{I}{V}$	The left side of MPP	Increase voltage until $V_{PV}=V_{MPP}$
Mode-3	$\frac{dP}{dV} < 0$	$\frac{\Delta I}{\Delta V} < -\frac{I}{V}$	Right Side of MPP	Decrease the voltage until $V_{PV}=V_{MPP}$

Table 5.2: Summary of the action by the Incremental Conduction algorithm [15]

5.3.3 Modified Incremental Conductance

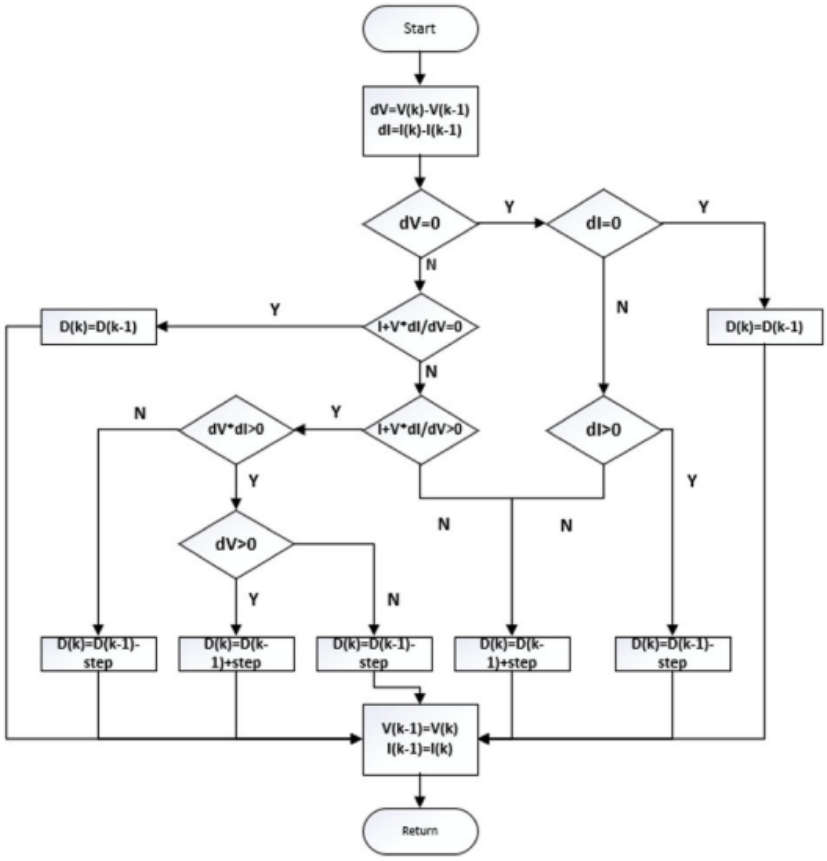

Figure 5.6: Modified IC flowchart [16].

The proposed algorithm is shown in the flow chart in figure 5.6 proposes to track both the maximum power point and the direction its going as opposed to the conventional method that only tracks the position of the maximum

power. When the solar irradiation suddenly increases, the operating point of the PV system moves in the positive direction. Therefore, both voltage and current increase. When the the voltage increase ($dv > 0$) and during this period while $dv > 0$, the duty cycle will continue to move in the direction of the previous step. So if the duty cycle was increasing it will continue to increase, whereas if the duty cycle was decreasing, it will continue to decrease. While for systems whose voltage decreases ($dv < 0$), the duty cycle will then move in the opposite direction of the previous step[16]. If the duty cycle was increasing it will begin to decrease, whereas if the duty cycle was decreasing, it will begin increasing. Similarly, the opposite holds true when the system is operating on the right side of the MPP and working in the positive running direction ($dv > 0$), the duty cycle will continue to move in the opposite direction of the disturbance of the previous step, behaving like the case for $dv < 0$ described above. Whereas for the negative system operating direction ($dv < 0$) and operating on the right hand side of the MPP, the duty cycle will continue to move in the direction of the disturbance of the previous step [16].

Chapter 6

Model Construction and case descriptions

6.1 Construction of the Models

To measure the effect of the irradiance on the solar cells and the power production, the simulation model is built using *Simulink*, available in *Matlab R2021a*. First by selecting the solar cell blocks available in the library and defining the cell in terms of the open circuit voltage and short circuit current respectively and defining the number of series cells per block, a subsection of the panel is formed. Each block represents 48 cells in series to form the submodule. Each module is composed of three subsections connected in series, with their own bypass diode connected in parallel as illustrated in figure 6.1. The parameters used for simulation of the solar cell block are summarized in table (6.1).

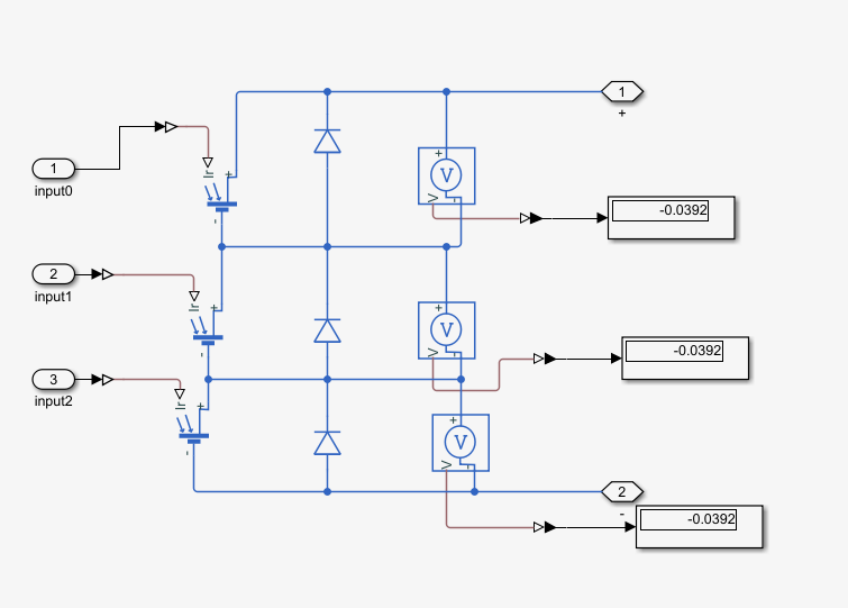

Figure 6.1: Solar cell blocks each representing 48 cells in series connected in parallel with the bypass diode 4.1.

Each solar module is connected to a converter block from the library. The converter operates based on the duty signal to alter the load within a range and it's parameters are summarized in table (6.2). In between the converter and the panel we connect an input capacitor in parallel. The voltage and the current of the module are measured and sent to the MPPT algorithm. The algorithm then outputs a duty cycle which is connected to the Pulse Width Modulator (PWM) generator, and the switch of the boost converter. The model is connected to an output resistance with sensors that allow the voltage and the current to be measured. The model, illustrated in figure (6.2 is capable of being scaled up to form a series array, like in figure (6.3). To compare both tracking at a module level and tracking at string level, an identical model, only instead of each module being connected to a converter, there is only one converter in the string.

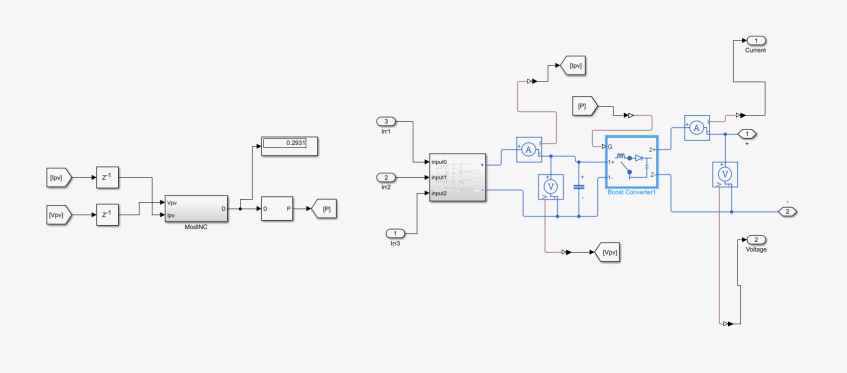

Figure 6.2: Solar Module (3×48 cells) in series connected to .

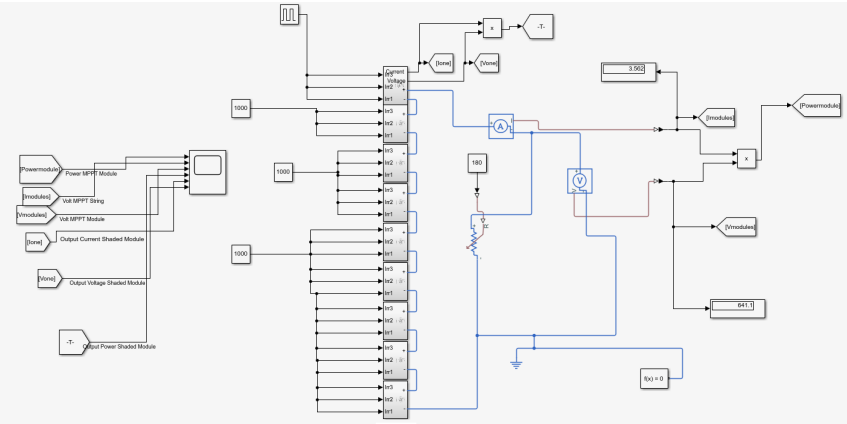

Figure 6.3: Full sized model of the system. Each subsystem includes one module and a boost converter configuration. 6.2

Table 6.1: Solar cell block parameters

Parameters	**Value**
Short-circuit Current I_{sc}	7.34 [A]
Open-circuit Voltage V_{oc}	0.6 [V]
Series Resistance R_s	0 [Ohm]
Quality factor	1.5
Number of cells in series N_s	48
Device Temperature T	25 [^oC]

Table 6.2: Module boost converter parameters

Converter Parameters	**Value**
Input Capacitance C_{in}	10 [μF]
Inductor L	0.5 [mH]
Output Capacitance C_{out}	1200 [μF]
Inductor resistance	0 [Ohm]
Output Capacitance resistance	0 [Ohm]
Diode off state conductance	1e-12 [$1/Ohm$]
Switch off state conductance	1e-12 [$1/Ohm$]
R_0	20 [Ohm]

Table 6.3: Boost converter parameters used for I.C.

Converter Parameters	**Value**
Input Capacitance C_{in}	500 [μF]
Inductor L	15 [mH]
Output Capacitance C_{out}	2200 [μF]
R_0	20 [Ohm]

6.2 Case Description:

The power a single solar cell produces is directly proportional to the area [28]. The first study case, Case 1.0, proposes to simulate different static partial shading conditions and obtain the I-V and P-V characteristic curves. The index a) through h) designate the different irradiance conditions simulated. Each submodule may have different irradiance levels identified by $"-"$. Each irradiance intensity corresponds to one subsection of the module unless it's uniform. Table 6.4 refer to the static conditions proposed to analyse.

For the effects of dynamic shading, one section of the module incumbent by one of the bypass diode has a step function whose amplitudes are 1000 W/m^2 and null, with each interval of time lasting for 0.5 *seconds*.

Static Case	index	Input [W/m^2]
1.0	a)	1000 uniform
	b)	800 uniform
	c)	600 uniform
	d)	400 uniform
	e)	200 uniform
	f)	1000-800-600
	g)	1000-600-400
	h)	1000-600-200
	i)	1000-1000-200
	j)	1000-1000-0
	k)	1000-0-0
	l)	200-0-0

Table 6.4: Case description for static conditions simulation

Case 2.0 Proposes to study the effect of the parameters of the boost converter for a fixed duty cycle. Each simulation is based on the reference in table 6.2, and the alterations are explained in table 6.5. Initially, the cases follow to understand the effect of the load and the duty cycle. The loads simulated vary from 4 *Ohm* to 60 *Ohm* under a fixed duty cycle of 0. and a 20 *Ohm* load a fixed duty cycle of 0.5 is compared (case a). Next, the duty cycle is fixed at 0.3 (reference) and compared with 0.7 (case b) and the values for the parameters of the boost converter are varied for the the inductor (case c), the input capacitor (case d), and the output capacitors (case e). The losses initially aren't taken into account. The losses from the series resistance of theses components are then measured, along with the internal conductance of the switch and diode elements, whose resistance we do not vary, (cases f through h).

Dynamic cases		Input: step 1000 and 0 [W/m^2] - (0.5 seconds each)	Duty Cycle	Description
2.0	a	1 submodule	Fixed at 0.4	Variation of Ro
			Fixed at 0.5	Ro = 20 Ohm
	b		Fixed at 0.3	Ro = 20 Ohm
			Fixed at 0.7	
	c		Fixed at 0.3	Variation of L
				Variation of Cout
				Variation of Cin
	d			Variation of L resistance
				Variation of Cout resistance
				Variation of Off state conductance
				of the switch and the diode

Table 6.5: Case description for dynamic conditions simulation

Then in case 3.0, three MPPT algorithms are applied and observed in terms of their power output performance. The three algorithms used are the

perturb and observe, the incremental conductance and the modified incremental conductance and are measured under different step sizes and duty ranges.

In case 4.0 the same dynamic function is applied to an entire module, and compares the module level MPPT control (without a string control) to a string level MPPT control, in a string of nine identical modules.

Chapter 7
Simulation Results

In this chapter, it is presented in the first subsection the results of the simulation and in the second subsection the discussion with the aid of literature.

7.1 Results

7.1.1 Case 1.0

The I-V curve and P-V curve for an operating temperature of 25 ℃ under different irradiation levels are illustrated in figures 7.1 and 7.2.

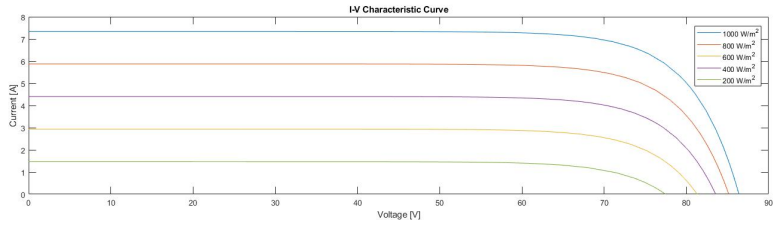

Figure 7.1: I-V characteristic curve for different levels off uniform irradiance

In figure 7.1 the blue curve represents case 1.0 *a*), and the green curve case 1.0 *e*). As can be seen, both the short-circuit current and open circuit voltage are diminished when the intensity of uniform irradiation is reduced. The short-circuit current is more affected by the change in irradiance and is the major contributor to the power difference under uniform conditions.

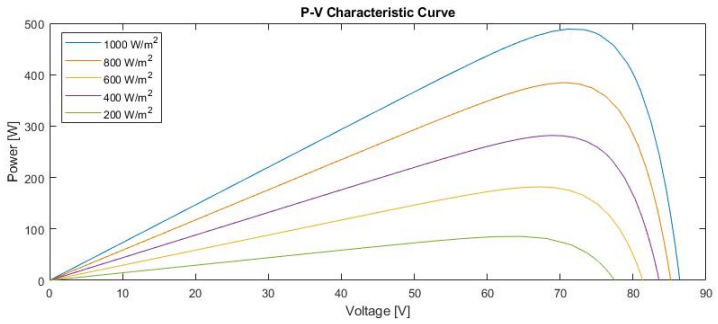

Figure 7.2: P-V characteristic curve for different levels of uniform irradiance

When the module is no longer uniformly irradiated and the submodules are under mismatched conditions, case 1.0 f) to h) the I-V develops steps in its curve while the P-V develops local and global peaks, as illustrated in figures , respectively. The results for case 1.0 are summarized in table 7.1 . The power percentage loss column compares the power output with the maximum achieved with a 1000 W/m^2 input uniform irradiance. As can be seen, the maximum available power when one module is completely shaded is about 63% of the maximum, just under two thirds. When two modules are totally shaded, the maximum power available represents only 26% of the maximum obtained. It is also preferable, up to a degree, to have a uniform irradiance then it is to have different levels of irradiance being applied to different sections of the panel, as can be seen for the cases of uniform 800 W/m^2 and 1000-800-600 W/m^2, where the power is greater for the case of uniform irradiance.

Input [W/m^2]	Current [A]	Voltage [V]	Power [W]	Rmp [Ohm]	Pecent loss
1000	6.73	72.62	488.53	10.79	100.00%
800	5.45	70.62	384.50	12.97	21.30%
600	4.08	69.14	281.86	16.96	42.30%
400	2.71	67.04	181.80	24.72	62.79%
200	1.35	63.47	89.70	47.02	82.46%
1000-800-600	4.29	74.32	318.46	17.35	34.81%
1000-600-400	2.86	74.15	212.06	25.93	56.59%
1000-600-200	4.23	47.70	201.61	11.29	58.73%
1000-1000-200	6.76	46.04	311.15	6.81	36.31%
1000-1000-0	6.72	45.97	309.00	6.84	36.75%
1000-0-0	6.56	19.52	128.03	2.98	73.79%
200-0-0	1.36	19.38	25.87	14.30	94.62%

Table 7.1: Summary of results obtained by shading one module under uniform and non-uniform irradiation

When analysing the results, the power output drops practically solely to the decrease in current caused by the decrease in irradiance. The voltage changes as well which can exacerbate the difference in power. Under non-uniform conditions, the position of the maximum power point doesn't always correspond to an increase in voltage. When one submodule is totally shaded the power output is zero for all the cells in series of that subsection, which

activates the bypass diode. As more submodules become shaded, the power output of the string begins to decrease.

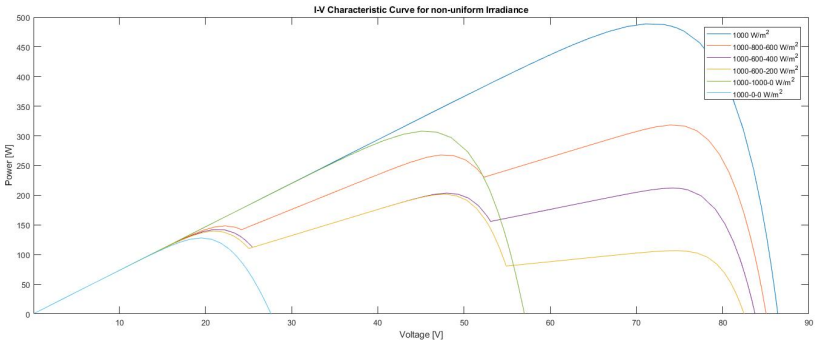

Figure 7.3: I-V characteristic curve for different levels of non uniform irradiance

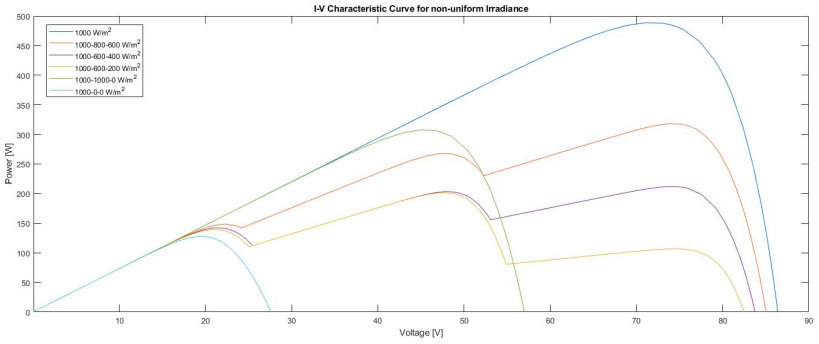

Figure 7.4: P-V characteristic curve for different levels of non uniform irradiance, case 1.0 a) and f) through k)

For the case of dynamic shading studied, the resulting P-V curves only have one maximum varying between $490W$ and $310W$ when fully illuminated and when one submodule is shaded in its entirety, respectively.

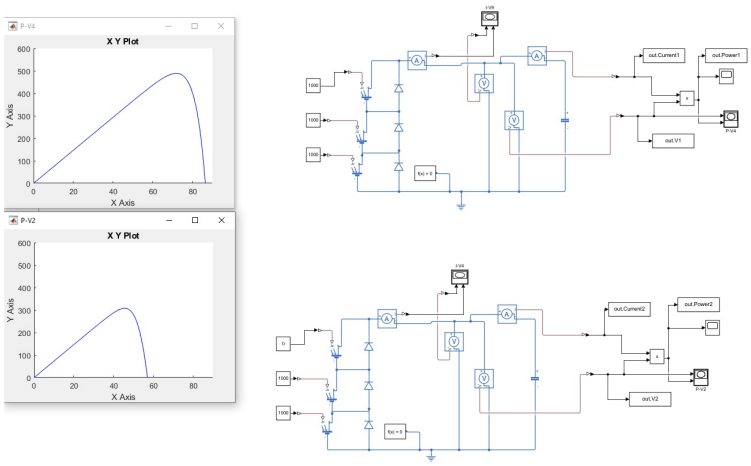

Figure 7.5: Model used for case 1.0. On the left side, the P-V graphs for the cases of uniform 1000 W/m^2 and the case 1000-1000-0 W/m^2 illustrate the variation of the characteristic curve if shading of one submodule takes place. On the right the model used to simulate case 1.0

7.1.2 Case 2.0

The following results refer to the cases descripted in 6.4.Figure 7.6 illustrates the response when the boost converter is subjected to a duty cycle of 0.4 under a switch frequency of 10000 Hz. The signl in red representing the the output power for a 20 Ohm resistance but with a fixed duty cycle of 0.5 and whose input capacitor has been ajusted to 100μF.

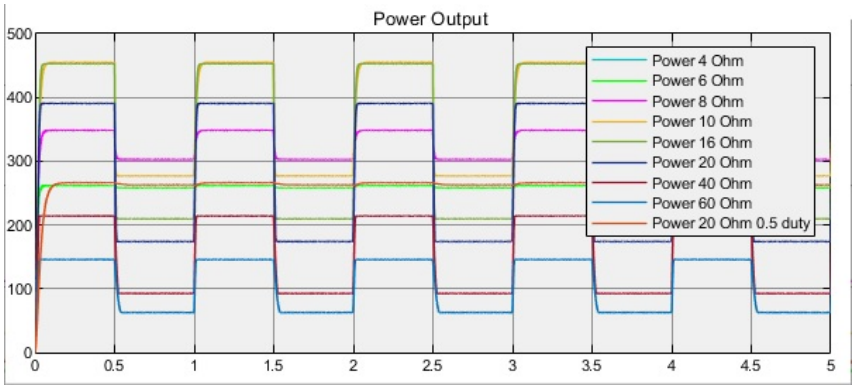

Figure 7.6: Power output vs time for different loads under dynamic shading of 1 subsection of 1 module

Here the power response of 4 Ohm was identical to that of 6 Ohm and very similar to the output power of 20 Ohm and 0.5 fixed duty cycle. For resistance values of 10 and 16 Ohm the system outputs around 450 W during maximum irradiation. However during the shaded periods, at 16 Ohm the maximum power is lower (210 W) compared to the 10 Ohm output resistance (280 W).

The reference output power signal is generated using the parameters in table 6.2 are represented in blue in figure 7.7. When increasing the duty cycle to 0.7, the power stagnates at around 100 W. When the value of the inductor increases, the output signal begins to develop overshoot and undershoot, along with an increase in the settling time. Varying the value too low leads to some steady state ripples and the maximum power during the uniform irradiated periods cannot be achieved.

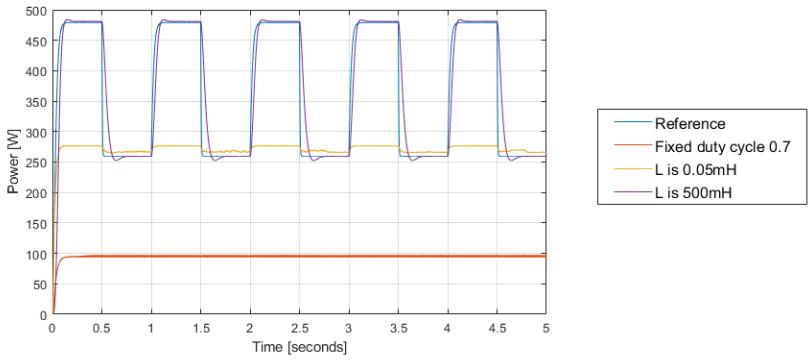

Figure 7.7: Power output vs time for different loads under dynamic shading of 1 subsection of 1 module

When varying the size of the input capacitor both the 10 μF and 16μF assist in achieving the maximum power but if it's values increase in magnitude too much, such as to 1000 μF then the maximum power begins decreasing as represented in yellow.

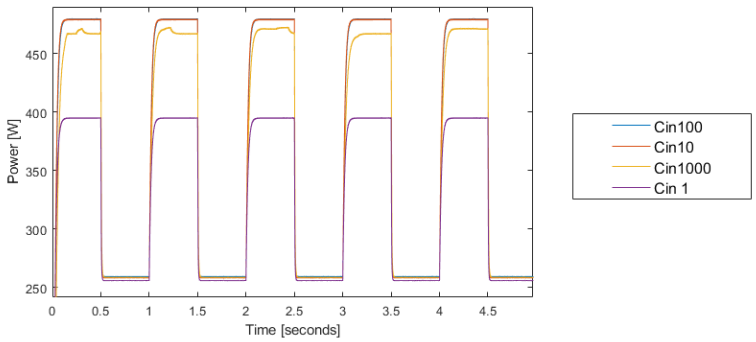

Figure 7.8: Changes to the magnitude of the power output signal for different values C_{in} [μF] and a fixed duty cycle under periodic shading

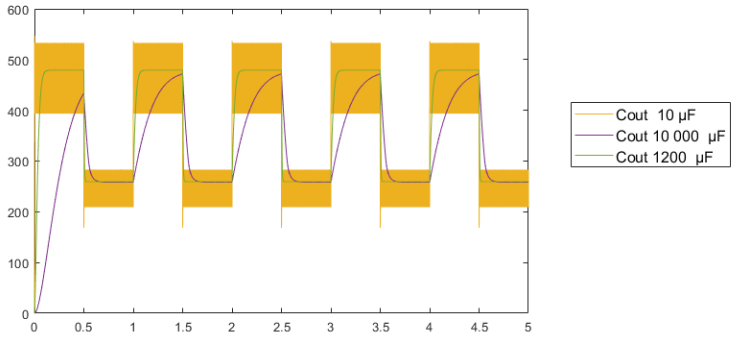

Figure 7.9: Changes to the ripple of the power signal for different values of C_{out} and a fixed duty cycle under periodic shading

In figure 7.9, for a very low capacitor value, the output signal develops large ripples. By increasing the size of the capacitor to 1200 μF the ripple diminishes significantly. As the size approaches 10000 μF, the maximum power can no longer be reached in the time interval when it is charging.

The Value of the inductor series resistance, figure 7.10 and the capacitor parallel resistance, figure 7.11,are components that add losses to the system and in case of the capacitor lead to some steady state ripple.

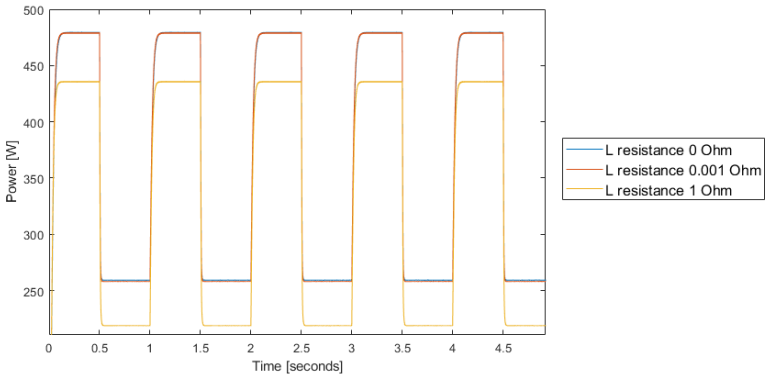

Figure 7.10: Changes to the magnitude of the power signal for different values of the inductor resistance and a fixed duty cycle under periodic shading

By increasing the series inductor resistance, the total output resistance is higher and the output power drops .

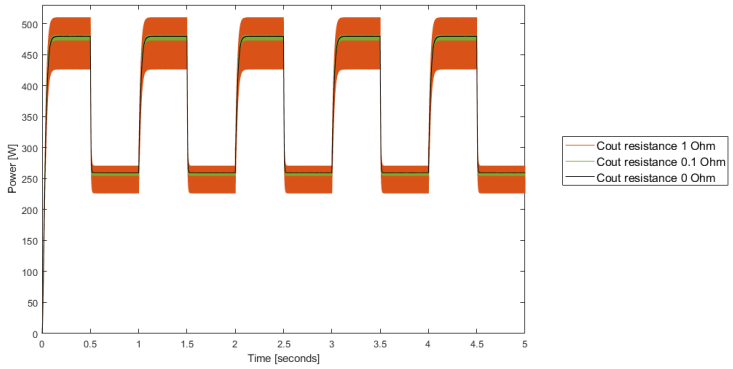

Figure 7.11: Changes to the output power signal for different values of C_{out} resistance and a fixed duty cycle under periodic shading.

When the resistance of the capacitor is too high, it begins introducing a big steady state power variation. In figure 7.12 the effect of the Off conductance of the switch and diode are presented.As the off conductance increases, the amount of energy stored by the inductor decreases.

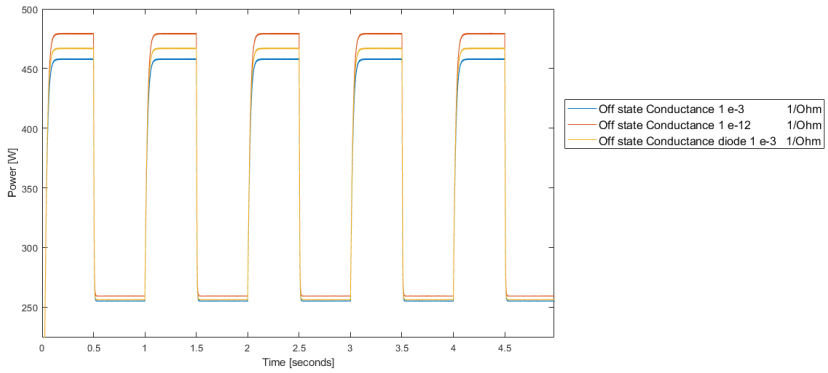

Figure 7.12: Changes to the magnitude of the power signal for different conductance values of the diode and the switch values and a fixed duty cycle under periodic shading

7.1.3 case 3.0

In case 3.0 the three algorithms simulated are perturb and observe, figure 7.13, the incremental conductance, figure 7.14 and a modified version of the incremental conductance 7.17.

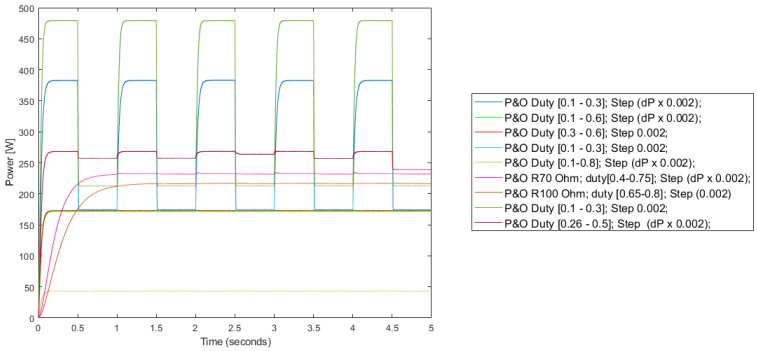

Figure 7.13: Simulation results of P&O algorithm under different duty ranges, step sizes and loads

By adjusting the duty cycle range, the output power signal can be adjusted for maximum power output or for a steady output, depending on the requirement. When the module is fully illuminated and the duty cycle's range is $[0.3 - 0.6]$ the output signal is nearly identical to when it's in the range $[0.1 - 0.6]$, suggesting that the upper boundary of the range, in this case 0.6 is responsible for adjusting the power under these irradiation conditions. When the upper boundary increases, the total amount of power decreases significantly. When the upper boundary is decreased the maximum amount of power generated during fully uniformly irradiated also increases.

In the P&O algorithm, the step size also has an effect on the amount generated. as when using a didn't allow for the system to operte at maximum power depending on the power performance output the difference in power was about 100 W for the dark blue and dark green curves and also may generate some fluctuation as demonstrated by the dark red output signal (duty cycle range $[0.26 - 0.5]$). When the load is adjusted, the duty cycle range is also adjusted to higher values, in contrast to what happens for the duty cycle range of $[0.1 - 0.8]$ which operates at around 47 W

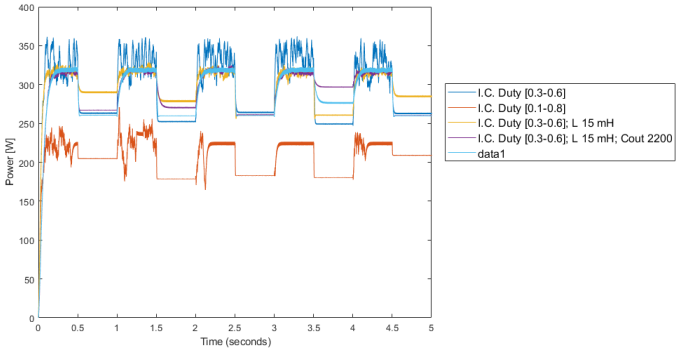

Figure 7.14: Simulation results of I.C. algorithm and further adjustment of converter

When simulating for a large duty cycle range, the Incremental conductance is able to output greater power, as is the case for the curve in orange

for a 20 Ohm output. resistance7.14. When the duty cycle range decreased the output power improved, however, displays a big fluctuation in the power requiring, an incease in the parameteres L, C_{out} and C_{in}, as illustrated in figure 7.15

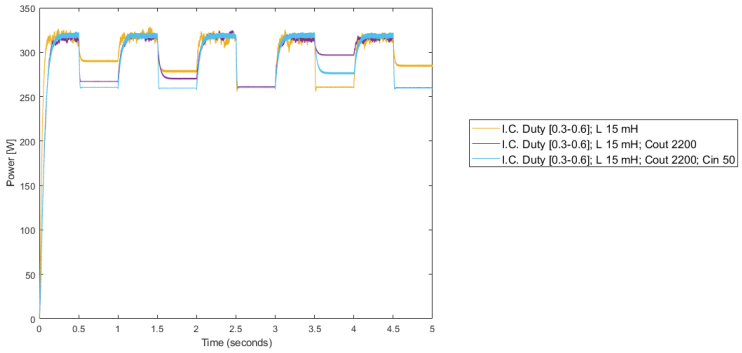

Figure 7.15: Simulation results for the Incremental Conductance algorithm

In figure 7.16, when the duty range was $[0.45 - 0.55]$, the power output varied by 10 W during the shading intervals. For the duty cycle ranges of $[0.28 - 0.35]$ (dark red) and $[0.3 - 0.6]$ (green), the upper boundary plays a significant factor in the total power generated during the fully irradiated periods. during the shaded intervals the systems output power is 250W in contrast to the 300W generated by the dark red curve.

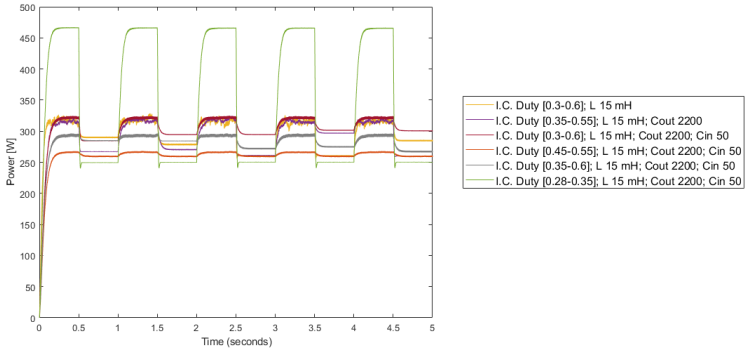

Figure 7.16: Simulation results of the Incremental Conductance algorithm: adjustment of the converter parameters

In the modified incremental conductance, the lower boundary of the algorithm seems to be responsible for the fully irradiated interval and the upper boundary for the shaded interval, in contrast to the P&O algorithm which works in the opposite fashion.

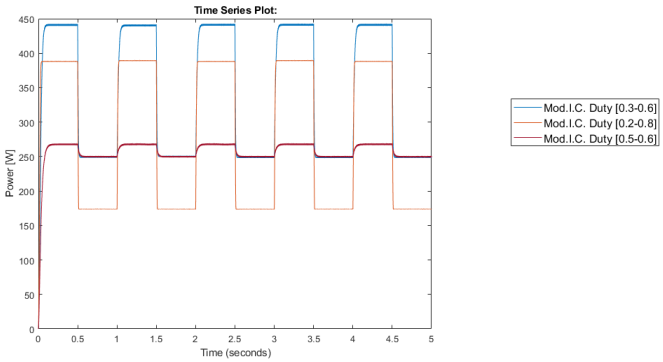

Figure 7.17: Simulation results of Modified Incremental Conduction, for different duty cycles

The step size of the duty cycle didn't alter much the behaviour of the signal. As the step size increases so does the final step between the duty range limit and the current value, which in return reduces marginally available range.

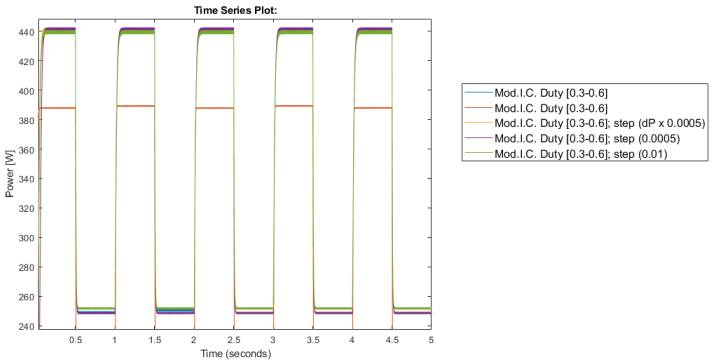

Figure 7.18: Simulation results of Modified Incremental Conduction, for different step sizes

In figure 7.18, the red curve refers to the duty cycle range between $[0.2 - 0.8]$ identical to figure 7.17

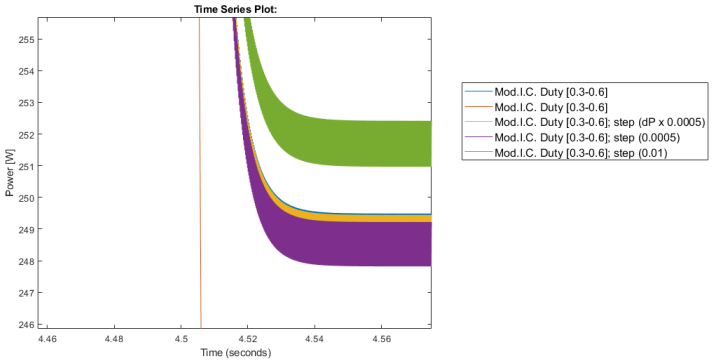

Figure 7.19: Close up view to the response for different step sizes

7.2 Discussion

When under different irradiation conditions, each submodule produced a different amount of power according to the amount of irradiance level, leading to more than one local maximum, each corresponding to one section encompassed by a diode. As the amount of shade increases, the MPP's begin to locate themselves very far from the normal MPP region and start depending more on the unshaded sections as discussed by [27]. The maximum power drop between the fully uniform 1000 W/m^2 irradiated condition and the $1000-1000-0$ W/m^2 is around 36% drop in the power generated.

To obtain the the maximum amount of power or a specific mitigated response for shading configurations depends on the load. There is a small range of loads that mitigate the effect of the dynamic output and can also be achieved by regulating the duty cycle. The resulting operating point comes from the intersection of the resistance and the I-V curve. As this points shifts, the system may become more or less sensitive towards the change in irradiance, depending on the value of the resistance and the power. When the load is adjusted to the maximum power at maximum irradiation, there is a greater discrepancy between the power at maximum irradiation and during the shaded interval. The system is more sensitive to shading. As the load increases, the power output becomes further more sensitive until the optimum load for maximum power is achieved. Beyond the maximum power point load the system becomes less sensitive to irradiation changes, (right hand side of the P-V curve). This is similar to what is explained in [49] where due to the power being delivered to the load being limited by the duty cycle, which acts like a control mechanism.

The parameters of the converter can be readily adjusted to tune the output signal in terms of the ripple, the component losses and response time. The inductor, which is mainly responsible for the voltage ripple, was also found to adjust the maximum power. An increase to it's value brought around a higher output, but also both overshoot and undershoot between shaded and non shaded states when the value went too high. The output capacitor was noted as the element that most mitigated the ripple effect on the load. If either of these parameters are too big, then the time it takes for the signal to track and reach the maximum power prolongs itself until it can no longer achieve the maximum value due to a lack of time between consecutive shading events. The parasitic elements like the inductor series resistance and the off-state conduction generates a loss in the power production. The output capacitor resistance contributes to some of the signal ripple and so when selecting the converter components a trade-off between the resistance they add, (and their effects on the system) and the magnitude of these components.

In terms of the converter, both the output capacitance and the inductance aid with the maintaining the voltage and current ripple within a desired range. If the values for the inductance and the output capacitance needed for continuous current mode are greater than those used, then the MPPT converter

cannot output a steady signal and may begin operating in the discontinuous current mode. The larger the output capacitance, the smaller the voltage ripple. Voltage ripple may also be reduced with a very large inductance. Nevertheless, By increasingly enlarging the capacitor, the solution starts generates a slow transient response and the settling time increases

It can be seen that the use of MPPT algorithms can improve the power under non ideal loads and irradiation conditions, as these algorithms are able to vary the duty cycle and alter the load, and in return the power signal [50].

The perturb and observe MPPT algorithm when it reaches the maximum power begins to oscillate very slightly, resulting in a slight power loss, and also suffers more when a quick change in irradiance takes place. However it is simple and easy to implement. In the simulations the amount of power extracted during the non shaded period was superior in the $P\&O$ algorithm, however during the shaded interval, as the irradiance lowers instantly, the power output is no longer the maximum power and is instead lower. No successful attempt at operating at the maximum power during both these irradiance configuration were achieved simultaneously when subjected to a sudden change in irradiation. There seems to indicate a compromise as the range of operation of this algorithm is limited under the stipulated dynamic shading conditions simulated. When subjected to a sudden change in irradiance, the $P\&O$ algorithm didn't achieve the maximum power during the shaded intervals and instead plateaus at a lower level. The incremental conductance algorithm in order to output a stable signal requires the inductor, the capacitor, or both to increase in size. Compared to the perturb and observe algorithm, however it suffers from a bigger ripple. due to the step size implemented being directly proportional to the active change in power means that the power output suffers a fluctuation while transiting periodically between the two irradiative states. The conventional INC algorithm fails to make a good decision when the irradiance is suddenly increased and the maximum power isn't achieved [10].

The modified version of the algorithm behaves similarly to the traditional variation, however offers a more accurate response without requiring additional resizing of the converter components. It seems to be slightly faster offering a reliable and accurate performance under rapidly changing irradiation. Although an improvment on the maximum power was observed relative to the conventional method, the power generated continue to be below the amount generated by using the $P\&O$ algorithm.

When trying a variable step increase such as dP $\times 0.02$, the power diminished also observed that if the optimum load falls outside the range of the duty cycle the MPPT algorithm doesn't show any improvement compared to a fixed duty cycle range. However when adjusted properly, the MPPT algorithm is able to output more power.

Comparing case 2.0 and 3.0 no improvements were observed under these instantaneous changing conditions between using a fixed duty cycle and a MPPT algorithm. In fact the power was lower or equal to the values generated by the fixed duty cycle.

Chapter 8
Conclusion

8.1 Conclusion

The effect of static shading on photovoltaics is an area that is well known. Interest in the behaviour and the limitations of reverse bias cells, have brought investigators to analyse solar cells with a high shunt resistance and a high reverse bias. By combining modules made up of cells with high shunt resistances, parallel bypass diodes and power optimisers it is hoped that the photovoltaic panels are able to respond to complex shading situations without signs of failure. For fast dynamic shading like that of a wind turbine or the passing of clouds, the abrupt changes to the states and the risk they pose to the system is an area which garners a lot of attention as hybrid solar wind parks become more prevalent and the transition from fossil fuels to more social and environmentally friendly sources of energy comes into full force. We conclude that the use of max power point tracking can improve the power output of modules and when adjusted properly, offer relatively simple control solutions which under a specific range of the duty cycle and load, permit a steady power output signal. By changing the duty cycle, the amount of power extracted can be optimised for the partial shading conditions it is experiencing. Under the partial shading conditions simulated, the $P\&O$ algorithm was able to reach the maximum power under fully illuminated conditions even when the load was beyond the optimum load. However, suffered more when under the partial shading condition. The incremental conductance algorithm required further resizing of the components of the converter and suffered from fluctuations in the power during the shaded and non-shaded events due to the variable step size. The modified incremental conductance was able to most accurately and reliably track the change in irradiance, though non of these incremental conductance algorithms were able to be adjusted in order to achieve maximum power as the module became fully illuminated. They both extracted more power during the shaded condition due to a more accurate tracking and control. The $P\&O$ algorithm is more simple and requires less complex hardware while the $I.C.$ algorithms and hardware implementation are more expensive.

Under these instantaneous changing conditions where the irradiation in one subsection of the module fluctuates between 1000 and 0 W/m^2 periodically

during a short interval, the power generated by using MPPT algorithms was lower or equal to the values generated by the fixed duty cycle.

8.2 Future Work

Having investigated the topic thus far, future interesting topics for research include a thermographic study in real conditions for exponential fitting and semi-empirical modeling approach to further understand the effects of shade. Implementing MPPT techniques alongside active reconfiguration techniques to perform estimative returns on investment and performance ratios and to further investigate mitigation techniques and solutions. Or the implementation of neural network control algorithms and other intelligent systems for further optimisation of the MPPT algorithms without the need for extra equipment. Utilize 3D graphical software integrated with graphic processing units to further quantify and solve complex shading problems such as the effects of dynamic shading

Bibliography

[1] https://www.pv-magazine.com/2020/08/27/south-koreas-largest-hybrid-solar-wind project/, “"pv-magazine: South korea’s largest hybrid solar-wind project",” 2020. Accessed on December 2020.

[2] B. Silva, M. Marques, and J. C. Matos, “Hibridização de parques eólicos: uma oportunidade para o setor.”

[3] I. Yahyaoui, Advances in Renewable Energies and Power Technologies, vol. 1. Jonathan Simpson, 2020.

[4] https://www.electronics-lab.com/article/pn-junction-theory/pn-junction-anatomy 2/, “"pv-magazine: South korea’s largest hybrid solar-wind project",” Accessed on December 2020.

[5] J. Svarc, “"solar panel construction",” 03 2020.

[6] M. Y. C. Ketchanji, E. S. Ndjakomo, I. A. Moukengue, et al., “A simple predictive performance model of solar cell under very hot and humide climate,” Journal of Power and Energy Engineering, vol. 7, no. 05, p. 26, 2019.

[7] S. Bowden and Honsberg.C, “https://www.pveducation.org/pvcdrom.”

[8] A. Luque and S. Hegedus, Handbook of Photovoltaic Science and Engineering. John Wiley Sons Ltd, 2003.

[9] https://components101.com/articles/introduction-to-different-types-of diodes, “Introduction to diodes: Basics, types, characteristics, applications packages,”

[10] S. Motahhir, e. g. Abdelaziz, S. Sebti, and A. Derouich, “Mil and sil and pil tests for mppt algorithm,” Cogent Engineering, vol. 4, 09 2017.

[11] https://ecowowlife.com/fill-factor-of-solar cell/, “Fill factor of solar cells,”

[12] M. Köntges, S. Kurtz, C. Packard, U. Jahn, K. Berger, K. Kato, T. Friesen, H. Liu, M. Van Iseghem, j. Wohlgemuth, D. Miller, M. Kempe, P. Hacke, F. Reil, N. Bogdanski, W. Herrmann, C. Buerhop, G. Razongles, and G. Friesen, “141212 iea-pvps t13-01 2014 review of failures of photovoltaic modules final 2014-05-06 bmwi logo,” 07 2015.

[13] Power Electronics - Converters, Applications, and Design.

[14] R. Ayop and C. W. Tan, "Design of boost converter based on maximum power point resistance for photovoltaic applications," Solar Energy, vol. 160, pp. 322–335, 2018.

[15] A. Ali, K. Almutairi, S. Padmanaban, V. Tirth, S. Algarni, K. Irshad, S. Islam, M. H. Zahir, M. Shafiullah, and M. Z. Malik, "Investigation of mppt techniques under uniform and non-uniform solar irradiation condition–a retrospection," IEEE Access, vol. 8, pp. 127368–127392, 2020.

[16] L. Shang, H. Guo, and W. Zhu, "An improved mppt control strategy based on incremental conductance algorithm," Protection and Control of Modern Power Systems, vol. 5, p. 14, 06 2020.

[17] ""cop26 verdict is governments urgently need to do more",," 2021.

[18] H. Mountford, D. Waskow, L. Gonzalez, C. Gajjar, N. Cogswell, M. Holt, T. Fransen, M. Bergen, and R. Gerholdt, "Cop26: Key outcomes from the un climate talks in glasgow," 2021.

[19] T. Benton, S. Bradley, A. Åberg, R. Townend, and N. Jeffs, "Cop26 verdict is governments urgently need to do more," 2021.

[20] NTPC, "Ntpc solar wind hybrid at kudgi - white paper on design approach for wind-solar hybrids."

[21] I. Mamia and J. Appelbaum, "Shadow analysis of wind turbines for dual use of land for combined wind and solar photovoltaic power generation," Renewable and Sustainable Energy Reviews, vol. 55, pp. 713–718, 2016.

[22] S. Guo, T. M. Walsh, A. G. Aberle, and M. Peters, "Analysing partial shading of pv modules by circuit modelling," in 2012 38th IEEE Photovoltaic Specialists Conference, pp. 002957–002960, IEEE, 2012.

[23] A. Sachenko[1], V. Kostylyov[1], V. Vlasiuk[1], I. Sokolovsky[1], and G. S. A. Perinparajah[2], "Development and implementation of a refined model for comprehensive characterization and optimization of highly efficient silicon solar cells," 2021.

[24] J. Carneiro and M. Passos, Sistemas Fotovoltaicos - Fundamento sobre Dimensionamento, vol. 1. Quântica Editora - Conteúdos Especializados, Lda., 2020.

[25] D. Giaffreda, M. Omaña, D. Rossi, and C. Metra, "Model for thermal behavior of shaded photovoltaic cells under hot-spot condition," in 2011 IEEE International Symposium on Defect and Fault Tolerance in VLSI and Nanotechnology Systems, pp. 252–258, IEEE, 2011.

[26] E. Bende, N. Dekker, and M. Jansen, "Performance and safety aspects of pv modules under partial shading: a simulation study," in Proceedings of the 29th European Photovoltaic Solar Energy Conference and Exhibition (EU PVSEC'14), 2014.

[27] R. Ahmad, A. F. Murtaza, H. A. Sher, U. T. Shami, and S. Olalekan, "An analytical approach to study partial shading effects on pv array supported by literature," Renewable and Sustainable Energy Reviews, vol. 74, pp. 721–732, 2017.

[28] A. Dolara, G. C. Lazaroiu, S. Leva, and G. Manzolini, "Experimental investigation of partial shading scenarios on pv (photovoltaic) modules," Energy, vol. 55, pp. 466–475, 2013.

[29] J. Wohlgemuth and W. Herrmann, "Hot spot tests for crystalline silicon modules," in Conference Record of the Thirty-first IEEE Photovoltaic Specialists Conference, 2005., pp. 1062–1063, IEEE, 2005.

[30] I. Geisemeyer, F. Fertig, W. Warta, S. Rein, and M. Schubert, "Prediction of silicon pv module temperature for hot spots and worst case partial shading situations using spatially resolved lock-in thermography," Solar Energy Materials and Solar Cells, vol. 120, pp. 259–269, 2014.

[31] D. Neuhaus, J. Kirchner, R. Mehnert, D. Sontag, J. Seerig, H. Hartmann, R. Lüdemann, and M. Eberspächer, "Impact of shunted solar cells on the iv characteristics of solar modules," in Proceedings of the 21st European Photovoltaic Solar Energy Conference (EU PVSEC'06), p. 2556, 2006.

[32] J. Teo, R. H. Tan, V. Mok, V. K. Ramachandaramurthy, and C. Tan, "Impact of partial shading on the pv characteristics and the maximum power of a photovoltaic string," Energies, vol. 11, no. 7, p. 1860, 2018.

[33] R. S. Anjos, R. Melício, V. M. Mendes, and H. M. Pousinho, "Crystalline silicon pv module under effect of shading simulation of the hot-spot condition," in Doctoral Conference on Computing, Electrical and Industrial Systems, pp. 479–487, Springer, 2017.

[34] G. Abdullah, H. Nishimura, and T. Fujita, "An experimental investigation on photovoltaic array power output affected by the different partial shading conditions," Energies, vol. 14, no. 9, p. 2344, 2021.

[35] L. Hassaine, E. OLias, J. Quintero, and V. Salas, "Overview of power inverter topologies and control structures for grid connected photovoltaic systems," Renewable and Sustainable Energy Reviews, vol. 30, pp. 796–807, 2014.

[36] R. K. Pachauri, O. P. Mahela, A. Sharma, J. Bai, Y. K. Chauhan, B. Khan, and H. H. Alhelou, "Impact of partial shading on various pv

array configurations and different modeling approaches: A comprehensive review," IEEE Access, vol. 8, pp. 181375–181403, 2020.

[37] G. S. Krishna and T. Moger, "Reconfiguration strategies for reducing partial shading effects in photovoltaic arrays: State of the art," Solar Energy, vol. 182, pp. 429–452, 2019.

[38] Ö. Çelik, A. Teke, and A. Tan, "Overview of micro-inverters as a challenging technology in photovoltaic applications," Renewable & Sustainable Energy Reviews, vol. 82, pp. 3191–3206, 2018.

[39] M. Madhukumar, T. Suresh, and M. Jamil, "Investigation of photovoltaic grid system under non-uniform irradiance conditions," Electronics, vol. 9, no. 9, p. 1512, 2020.

[40] D. D. Nguyen, "Modeling and reconfiguration of solar photovoltaic arrays under non-uniform shadow conditions," 2008.

[41] S. Gallardo Saavedra, "Analysis and simulation of shading effects on photovoltaic cells," 2016.

[42] N. Dekker, M. Jansen, A. Burgers, M. Dörenkämper, R. Jonkman, R. van der Ven, and E. Gramsbergen, "Selective deployment of power optimizers: effect of shade on performance and hotspots in pv modules," in 37th EUPVSEC European PV Solar Energy Conference and Exhibition, 7-11 September 2020, Lisbon, Portugal, WIP GmbH & Co Planungs-KG, 2020.

[43] B. Newman, A. Burgers, N. Dekker, P. Manshanden, M. Jansen, and J. Kester, "Impact of dynamic shading in csi pv modules and systems for novel applications," in 2019 IEEE 46th Photovoltaic Specialists Conference (PVSC), pp. 3088–3092, IEEE, 2019.

[44] M. A. Ramli, S. Twaha, and Z. Al-Hamouz, "Analyzing the potential and progress of distributed generation applications in saudi arabia: The case of solar and wind resources," Renewable and sustainable energy reviews, vol. 70, pp. 287–297, 2017.

[45] J. Robledo, J. Leloux, B. Sarr, C. A. Gueymard, and P. Darez, "Dynamic simulation of the shading cast by a wind farm on an adjacent photovoltaic plant,"

[46] D. Jena and V. V. Ramana, "Modeling of photovoltaic system for uniform and non-uniform irradiance: A critical review," Renewable and Sustainable Energy Reviews, vol. 52, pp. 400–417, 2015.

[47] M. T. Ahmed, T. Gonçalves, A. Albino, M. R. Rashel, A. Veiga, and M. Tlemcani, "Different parameters variation analysis of a pv cell," in 2016

International Conference for Students on Applied Engineering (ICSAE), pp. 176–180, IEEE, 2016.

[48] S. Kasbi, E. Rijanto, and R. bin Abd Ghani, "Design and implementation of controller for boost dc-dc converter using pi-lpf based on small signal model," Mechatronics, Electrical Power & Vehicular Technology, vol. 6, no. 2, 2015.

[49] A. Sangwongwanich, Y. Yang, and F. Blaabjerg, "Development of flexible active power control strategies for grid-connected photovoltaic inverters by modifying mppt algorithms," in 2017 IEEE 3rd International Future Energy Electronics Conference and ECCE Asia (IFEEC 2017-ECCE Asia), pp. 87–92, IEEE, 2017.

[50] U. Srikanth, P. P. Kumar, and K. Prasad, "A comprehensive comparison of mppt algorithms with dc-dc converters for solar pv array," Journal of Emerging Technologies and Innovative Research, vol. 4, no. 9, pp. 41–52, 2017.